

Article

Tracing the Origin and Magmatic Evolution of the Rejuvenated Volcanism in Santa Clara Island, Juan Fernández Ridge, SE Pacific

Javier Reyes ^{1,*} , Luis E. Lara ^{2,3} , Vanessa Sutherland ⁴, Nicolás Aguirre ⁴, Carlos Orellana ⁴, Folkmar Hauff ⁵  and Kaj Hoernle ^{5,6}

¹ Escuela de Ciencias del Mar, Pontificia Universidad Católica de Valparaíso, Valparaíso 2373223, Chile

² Instituto de Ciencias de la Tierra, Facultad de Ciencias, Universidad Austral de Chile, Valdivia 5090000, Chile

³ CKELAR Instituto Milenio de Investigación en Riesgo Volcánico, Antofagasta 1270709, Chile

⁴ Independent Researcher, Santiago 8320000, Chile

⁵ GEOMAR Helmholtz Centre for Ocean Research Kiel, 24148 Kiel, Germany

⁶ Institute of Geosciences, Kiel University, 24118 Kiel, Germany

* Correspondence: javier.reyes@pucv.cl or javier.reyes87@gmail.com

Abstract: Oceanic intraplate volcanoes sometimes experience late-stage eruptive activity known as rejuvenated volcanism, and contrasting interpretations for its petrogenesis depend on the compositional characteristics. In the Juan Fernández Ridge (JFR), a volcanic chain approximately 800 km in length emplaced on the Nazca Plate, some subaerial occurrences of rejuvenated volcanism have been recognized on the Robinson Crusoe and Santa Clara Islands, both part of the same deeply eroded shield volcano complex. This study aims to understand the origin and magmatic evolution of rejuvenated volcanism on Santa Clara Island, emplaced after ~2.15 Ma of quiescence above the shield sequence, mainly via the analysis of unpublished geochemical and isotopic data. Field reconnaissance identified two nearly coeval rejuvenated sequences on Santa Clara Island: Bahía W (BW) and Morro Spartan (MS), both formed by basanitic and picro-basaltic lava flows with brecciated levels and local intercalations of sedimentary and pyroclastic deposits. In comparison to the chemical signature of the preceding shield-building stage (comprised mainly of basalts and picrites), the two rejuvenated sequences exhibit a notable enrichment in incompatible elements, but the Sr, Nd, and Pb isotopes are very similar to the FOZO mantle endmember, with an apparent additional contribution of HIMU and EM1 components. The geochemistry of lavas revealed the involvement of various processes, including contamination by ultramafic xenoliths, high-pressure fractional crystallization of olivine and clinopyroxene, and potential partial assimilation of oceanic lithospheric components. While the oceanic lithosphere has been considered as a potential source, the isotopic data from Santa Clara lies outside of the mixing curve between depleted mantle (DM, here represented by the North Chile Rise and the East Pacific Rise) and the previous shield stage, suggesting that a lithospheric mantle is not the primary source for the rejuvenated stage volcanism. Therefore, we favor an origin of the rejuvenated volcanism from the mantle plume forming the JFR, supported by similarities in isotopic signatures with the shield stage and high values of $^{208}\text{Pb}/^{204}\text{Pb}$ (only comparable to San Félix—San Ambrosio in the vicinity of JFR), implying the presence of a regional source with radiogenic $^{208}\text{Pb}/^{204}\text{Pb}$ isotope ratios. In addition, isotopic variations are subparallel to the mixing line between HIMU and EM1 components, whose participation in different proportions might explain the observed trends. In conclusion, we propose that the source of the rejuvenated volcanism on Santa Clara Island is a heterogeneous mantle plume, the same one that fed the shield stage. The rejuvenated volcanism is derived from a secondary melting zone away from the main axis of the plume.

Keywords: Juan Fernández; Santa Clara Island; Sr-Nd-Pb isotopes; rejuvenated volcanism; mantle plume; mantle heterogeneities



Citation: Reyes, J.; Lara, L.E.; Sutherland, V.; Aguirre, N.; Orellana, C.; Hauff, F.; Hoernle, K. Tracing the Origin and Magmatic Evolution of the Rejuvenated Volcanism in Santa Clara Island, Juan Fernández Ridge, SE Pacific. *Minerals* **2024**, *14*, 524.

<https://doi.org/10.3390/min14050524>

Received: 2 April 2024

Revised: 15 May 2024

Accepted: 16 May 2024

Published: 19 May 2024



Copyright: © 2024 by the authors. Licensee MDPI, Basel, Switzerland. This article is an open access article distributed under the terms and conditions of the Creative Commons Attribution (CC BY) license (<https://creativecommons.org/licenses/by/4.0/>).

1. Introduction

Oceanic intraplate volcanism is typically characterized by the formation of voluminous shield volcanoes, both subaerial and submarine, composed of ocean island basalts (OIB) with a geochemical composition generally enriched compared to mid-ocean ridge basalts (MORB). Sometimes, OIB-type volcanism gives rise to chains of oceanic islands and seamounts that display an age progression concordant with the movement of the underlying oceanic plate (first described for Hawaii by [1,2]). In such cases, the origin is often associated with the ascent of mantle plumes to the asthenosphere–lithosphere boundary, where they melt and form magmas that feed the volcanoes emplaced above [3,4]. However, in some intraplate settings, the presence of low volumes of more silica-undersaturated volcanism with ages younger than and often separated by a volcanic hiatus from the shield stage has been recognized (Hawaii, Samoa, Juan Fernández Ridge, among others) (e.g., [5–9]), which is not entirely consistent with the mantle plume theory in its simplest formulation. This late magmatic stage is known as rejuvenated volcanism, and its products are characterized by petrographical, geochemical, and isotopic signatures distinct from shield lavas, typically being more alkaline and with relatively depleted isotopic ratios [10]. This permitted contrasting interpretations of the mantle source, either more enriched or depleted than in earlier stages, depending on the case under study and probably related to the great variety of specific cases grouped under the concept of rejuvenated volcanism.

For example, the archetypal case of Hawaii is characterized by a relatively brief volcanic quiescence between shield and rejuvenated stages, with the latter more alkaline and depicting isotopic signatures indicative of slightly more depleted sources (e.g., [10,11]). This has led to interpretations of the origin, either of late melting of the same mantle plume that fed the previous shield stage, possibly zoned or with compositional heterogeneities [12–14], or by melting of a metasomatized oceanic lithosphere [15,16]. Other cases such as Mauritius, exhibit signatures interpreted as characteristic of the same mantle plume that formed the shield volcanism [17]. In the Canary Islands, geochemical studies support the origin of the rejuvenated (post-erosional) volcanism via the interaction of plume-derived melts with the asthenosphere [18–20] and the lithospheric mantle [21]. However, in other tectonic settings like the Selvagen Islands, isotopic signatures and prolonged volcanic inactivity after the shield stage suggest a predominantly lithospheric mantle source [22]. The latter is similar to Samoa, where the geochronological variation is not as pronounced, which could be a result of the passage of the lithosphere above other mantle plumes capable of modifying the isotopic composition of the lithosphere, thus generating a signature different from the shield [7]. This might suggest that each deserves its own explanation, and it seems to be challenging to reconcile all these expressions with a common driving process and/or a single petrogenetic model.

In the Nazca Plate, SE Pacific, rejuvenated volcanism has only been reported on the Juan Fernández Ridge (JFR) [8,9,23], whose shield stage was formed by a slightly heterogeneous mantle plume [24–28]. Rejuvenated volcanism has been reported for Robinson Crusoe Island [8,23] and O'Higgins Guyot [9]. However, the limited amount of available data does not allow us to fully elucidate the genesis of the rejuvenated volcanism, which seems to be a persistent and ubiquitous process along the JFR. This contribution provides data on Santa Clara Island at JFR, where more extensive reconnaissance exists about the occurrence of a late stage of volcanism and aims to assess the viability of genetic models (either a mantle plume, asthenosphere, and/or metasomatized oceanic lithosphere) by analyzing new geochemical and isotopic data along with previously published mineral chemistry data [8].

2. Geological Background

The JFR is a volcanic chain including three main islands, from east to west: Robinson Crusoe, Santa Clara (both parts of the same deeply eroded shield volcano complex), and Alejandro Selkirk, along with at least 12 seamounts [29] (Figure 1). This ca. 800 km long chain is emplaced on the Nazca Plate, which migrates towards the South American Plate

with a velocity of approximately ~ 70.5 mm/yr [29]. Santa Clara is a small ca. 2.2 km² island where detailed mapping [30] allowed early recognition of an upper sequence lying unconformably above a gently dipping sequence of pahoehoe lavas typical of the shield stage. More recently, extensive $^{40}\text{Ar}/^{39}\text{Ar}$ dating provided the age of the upper sequence in the range of ~ 1.25 – 0.90 Ma [23] and provided a more stratigraphic context for the so-called Volcanes de Santa Clara [23], the local expression of the rejuvenated stage. In detail, this unit is a gently dipping sequence up to 180 m thick, composed of a basal section formed by basanitic lavas and conglomerates and an upper section dominated by thick lava flows.

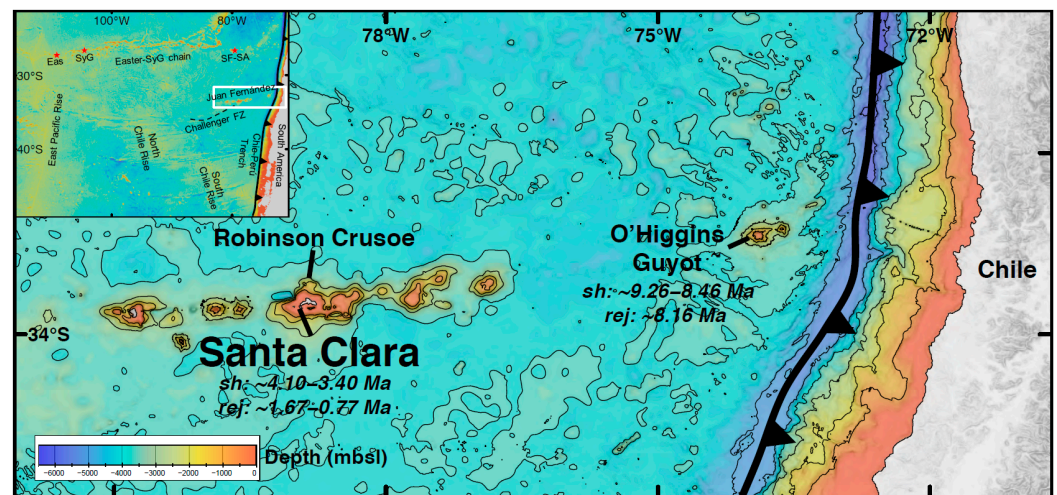


Figure 1. Bathymetric map of the Juan Fernández Ridge on the Nazca Plate (modified from [28]). The three locations where rejuvenated volcanism has been recognized are highlighted, from E to W: O'Higgins Guyot, Robinson Crusoe, and Santa Clara Islands. The $^{40}\text{Ar}/^{39}\text{Ar}$ age ranges for the shield (sh) and rejuvenated (rej) stages are also shown [8,9,23,29]. The inset shows the locations of major oceanic bathymetric features and islands (Eas: Easter, SyG: Salas y Gomez, SF-SA: San Félix and San Ambrosio) around the JFR.

Previous petrological studies suggest that volcanism along the JFR is related to the melting of a slightly heterogeneous mantle plume with apparently low potential temperatures, high $^3\text{He}/^4\text{He}$ isotopic ratios in some cases, and a well-developed age progression [24–29], ranging from ~ 9.26 Ma in the east (Guyot O'Higgins) to ~ 0.62 Ma in the west (Friday Seamount) [29]. Shield volcanoes at the JFR are predominantly composed of transitional basalts, picrites, and meimequites with a Sr-Nd-Pb isotopic signature close to the common FOZO (FOcal ZONE) mantle endmember, with additional contributions from enriched mantle 1 (EM1) and high μ (HIMU) components [28] (see [31–35] for more general information on mantle components). Based on geological, geochronological, and geochemical criteria and following a variable period of magmatic quiescence, rejuvenated volcanism has been reported in at least two volcanic complexes at the JFR, from east to west, the Guyot O'Higgins [9] and the Robinson Crusoe/Santa Clara Islands [8,23]. The Guyot O'Higgins revealed a morphology interpreted as a lava flow with a radiometric age of ~ 8.16 Ma [9] superimposed on a shield volcano (~ 9.26 – 0.77 Ma [9]), as evidenced by bathymetric and backscatter information [9]. For the Robinson Crusoe and Santa Clara Islands, mapping at 1:25,000 has recognized and dated outcrops in the range of ~ 1.67 – 0.77 Ma that were assigned to at least 6 and 2 different vents, respectively [8,23]. These ages are considerably younger than the shield stage, dated by $^{40}\text{Ar}/^{39}\text{Ar}$ between ~ 4.10 and ~ 3.40 Ma [8,9,23,29]. Samples from these units present compositional characteristics very similar to those reported for the O'Higgins Guyot [9], which collectively describe the features of the rejuvenated stage at JFR. The limited existent data implies that rejuvenated lavas consist of basanites and picrites with scarce presence of ultramafic xenoliths [8,23]. Geobarometry of selected samples from Robinson Crusoe Island indicates

rapid ascent of rejuvenated basanitic/picritic magmas. Some samples with high MgO content experienced polybaric crystallization of olivine and clinopyroxene, while others, slightly more differentiated, were stored briefly in transient reservoirs [8]. Regarding the mantle source, Ref. [27] proposes the influence of metasomatized lithosphere based on Os isotopes, although the signature is very similar to the shield and shows a significant range of variability.

3. Sampling and Analytical Procedures

To expand earlier studies in order to obtain a more comprehensive picture of the rejuvenated volcanism in Robinson Crusoe and Santa Clara Islands, in March 2023, geological fieldwork and aerial photography using a drone were conducted to select sampling sites for relatively fresh rocks based on stratigraphic criteria. A total of 10 lava samples were collected in Santa Clara, which adds to 8 rocks sampled in a previous exploratory campaign in 2012. Petrographic analysis of these samples was conducted using an optical microscope, along with a modal count of 500 points, performed with JMicroVision 1.2.7 software. This was complemented with mineral chemistry data for a previously published sample [8]. In summary, the chemistry of olivine and clinopyroxene was analyzed using an electronic microprobe (EPMA JEOL JXA 8230 (Peabody, MI, USA) with three wavelength-dispersive spectrometers) at the Electron Microscopy and X-ray Analysis Laboratory (LAMARX), Universidad Nacional de Córdoba, Argentina. The crystals TAP (Na, Mg, Al, and Si), PET (Ca and Ti), and LiF (Cr, Mn, Fe, and Ni) were used for analysis under an accelerating potential of 15.0 kV and an electron beam current of 20 nA in 5 μm circles. Counting times were 10 s for peaks and 5 s at each background position, with data reduction performed using the ZAF correction method.

Whole-rock geochemical analyses for the 18 samples were performed in two different batches (2012 and 2023) but following the same analytical procedures by the AcmeLabs of Bureau Veritas in Vancouver, BC, Canada (<https://commodities.bureauveritas.com/metals-minerals/exploration-and-mining/geoanalytical-services> accessed on 17 May 2024). Pretreatment of the samples was carried out by the authors first crushing in a portable ASC Scientific Laboratory Jaw Crusher to reduce to 2–3 mm and then pulverized until 85% passed through a 200-mesh sieve (<0.074 mm). Once in the laboratory, separate aliquots were mixed with lithium metaborate/tetraborate for major element analysis using inductively coupled plasma emission spectroscopy (ICP-OES) and digested with dilute nitric acid for trace element analysis using inductively coupled plasma–mass spectrometry (ICP-MS). Another split was digested in aqua regia and analyzed by ICP-MS for a more precise measurement of Ni and Pb contents. Loss on ignition (LOI) was determined by weight comparison after ignition at 1000 °C. Detection limits vary between 0.01 to 0.04 wt% for major elements and between 0.01 and 1 ppm for trace elements (details in Table 1). Analytical precision and accuracy were verified based on duplicate analyses and internal laboratory standards, with values generally below 1% and 2% for major elements and less than 10% for trace elements (except for some oxides and elements such as P₂O₅ and Pb, with slightly higher values).

Table 1. Concentrations of major (wt%) and trace (ppm) elements in samples from the rejuvenated volcanism on Santa Clara Island. Fe₂O₃^T: total iron as ferric iron. LOI (wt%) is included. (*) Major elements taken from [8].

Sample	SiO ₂	TiO ₂	Al ₂ O ₃	Fe ₂ O ₃ ^T	MgO	MnO	CaO	Na ₂ O	K ₂ O	P ₂ O ₅	Ni	LOI	Sum	Cr ₂ O ₃	Sc	Ba	Co	Ga	Hf	Nb	Rb	Sr	Ta	Th	U	V	Zr	Y	Pb	La	Ce	Pr	Nd	Sm	Eu	Gd	Tb	Dy	Ho	Er	Tm	Yb	Lu
Det. Limit	0.01	0.01	0.01	0.04	0.01	0.01	0.01	0.01	0.01	0.01	0.1	0.1		0.002	1	1	0.2	0.5	0.1	0.1	0.1	0.5	0.1	0.2	0.1	8	0.1	0.1	0.1	0.1	0.1	0.02	0.3	0.05	0.02	0.05	0.01	0.05	0.02	0.03	0.01	0.05	0.01
Bahía W (BW)																																											
SCL-06	42.38	2.72	12.78	12.12	11.53	0.23	10.19	3.62	1.61	0.76	242.4	1.4	99.55	0.070	21	575	50.8	19.1	7.0	81.5	48.8	865.2	4.8	7.5	1.8	279	327.4	30.2	3.0	61.9	118.5	13.94	53.3	9.64	3.05	8.40	1.20	6.17	1.12	2.80	0.37	2.14	0.29
LL230112-4 (*)	43.00	2.80	12.91	11.74	11.45	0.18	11.51	2.42	0.55	0.53	257.5	2.2	99.43	0.104	30	644	76.7	24.6	7.4	84.1	7.9	999.0	5.1	7.0	1.6	441	324.9	36.0	1.9	58.7	117.4	13.54	56.4	10.90	3.43	10.77	1.30	7.67	1.31	3.23	0.44	2.92	0.40
SCL-05	41.40	2.86	12.80	12.58	12.54	0.19	10.58	2.62	1.32	0.62	236.2	1.9	99.57	0.071	25	486	59.3	18.5	5.8	65.9	36.5	737.6	3.8	5.8	1.5	314	256.3	27.1	1.5	48.3	89.6	10.85	42.2	7.62	2.42	7.15	1.04	5.37	1.01	2.63	0.37	2.04	0.30
SCL-01	42.08	3.15	13.64	12.84	10.66	0.20	10.64	3.25	1.52	0.61	190.3	0.9	99.58	0.054	25	534	50.3	16.6	6.3	66.6	41.1	764.8	4.0	6.4	1.6	300	272.2	28.4	2.1	47.6	93.1	11.05	43.1	8.25	2.63	7.46	1.07	5.77	1.07	2.82	0.37	2.15	0.30
SCL-04	42.24	3.07	13.15	12.49	11.96	0.19	9.77	2.95	0.90	0.59	269.0	2.1	99.56	0.066	24	510	55.3	16.0	6.0	64.3	23.3	758.8	4.1	5.9	1.2	288	262.5	26.9	1.3	46.0	90.9	10.73	41.9	8.36	2.57	7.09	1.03	5.83	1.00	2.90	0.36	2.16	0.29
SCL-03	41.70	3.31	13.57	13.44	10.82	0.20	9.77	2.81	0.78	0.63	247.6	2.4	99.57	0.053	23	556	54.1	16.3	6.5	66.7	25.2	783.3	4.2	6.3	1.4	302	274.1	27.5	1.2	49.3	92.7	11.07	43.3	8.10	2.64	7.39	1.07	5.75	1.06	2.77	0.37	2.21	0.30
LL230112-2 (*)	41.32	2.73	12.58	12.75	13.31	0.19	10.31	2.43	1.33	0.58	273.1	1.7	99.39	0.072	25	678	82.4	22.4	7.6	88.5	47.4	1038.0	5.3	7.8	1.9	385	326.9	36.7	2.1	62.0	118.3	14.13	58.4	10.48	3.39	10.58	1.29	7.87	1.35	3.20	0.45	2.79	0.41
JR230112-2 (*)	41.42	3.34	13.62	13.69	8.66	0.21	10.77	3.93	0.68	0.61	154.2	2.6	99.57	0.056	28	530	54.9	18.5	5.8	71.9	46.9	807.8	4.0	5.0	1.5	278	257.2	28.6	0.4	48.0	91.2	10.81	42.4	8.18	2.50	7.59	1.11	5.84	1.06	2.75	0.40	2.40	0.33
JR230112-1 (*)	42.19	3.18	13.10	13.10	11.04	0.20	10.78	3.88	0.78	0.61	172.5	0.6	99.53	0.058	28	535	53.9	18.8	6.5	72.1	38.3	813.3	3.8	5.5	1.2	312	262.3	28.1	1.2	49.4	93.8	11.14	45.4	8.16	2.61	7.77	1.14	6.48	1.08	2.97	0.39	2.54	0.32
JR160913-2 (*)	42.66	3.06	14.32	12.98	8.96	0.22	10.28	3.37	0.99	0.72	132.9	1.9	99.50	0.049	25	762	49.5	18.1	6.9	76.1	11.4	962.5	4.8	7.0	1.5	276	299.6	30.8	2.6	59.8	113.8	13.24	51.2	9.26	2.87	8.25	1.23	6.48	1.27	3.21	0.46	2.81	0.41
Morro Spartan (MS)																																											
MSP-04	42.81	2.91	13.62	13.43	9.28	0.22	9.92	3.57	1.64	0.91	143.5	1.1	99.58	0.048	23	578	46.2	16.8	7.7	77.7	47.1	873.7	4.9	7.6	1.8	245	338.5	32.8	3.1	61.4	115.3	13.98	53.0	9.99	3.10	8.83	1.24	6.68	1.23	3.14	0.44	2.67	0.37
JR230112-3 (*)	42.99	2.91	13.43	13.77	9.52	0.23	9.81	3.79	1.70	0.91	142.4	0.4	99.51	0.048	22	625	46.4	18.6	8.0	86.4	50.7	974.5	5.1	7.6	2.0	231	345.5	32.5	3.0	61.3	118.3	13.63	52.0	9.94	3.16	9.19	1.28	7.00	1.30	3.31	0.47	2.83	0.39
MSP-03	41.84	3.25	13.90	13.61	8.69	0.22	10.29	3.67	1.85	0.86	111.1	1.3	99.59	0.032	21	588	44.9	17.4	7.1	77.0	51.2	856.9	4.8	7.3	1.6	279	315.0	32.4	2.2	58.7	112.8	13.58	52.0	9.72	3.05	8.69	1.26	6.50	1.20	3.32	0.42	2.66	0.35
MSP-02	41.05	3.46	13.75	13.30	9.52	0.21	10.68	3.26	0.79	0.66	111.2	2.8	99.58	0.037	25	648	48.9	17.8	7.0	78.0	25.0	894.0	4.8	7.0	1.6	304	300.0	30.3	2.5	57.7	109.6	13.07	51.6	9.52	3.07	8.62	1.19	6.37	1.17	3.06	0.38	2.54	0.34
MSP-01	40.75	3.54	13.60	13.82	9.64	0.21	10.46	2.87	1.01	0.66	109.8	2.9	99.58	0.036	25	680	51.1	17.1	6.8	76.6	18.3	869.3	4.7	6.9	1.6	311	288.0	30.4	1.8	55.3	107.1	12.90	49.5	9.32	2.99	8.03	1.16	6.30	1.20	3.12	0.38	2.50	0.34

The methodology for measuring isotopic ratios is outlined in [28] (analyzed within the same set of samples). In brief, isotopic analyses of Sr, Nd, and Pb were conducted on 3 rock samples. Prior to acid digestion, rock fragments (100–150 mg from the 0.5–2 mm fraction) underwent leaching in 2 N HCl at 70 °C for 1–2 h, followed by three rinses with 18.2-M Ω water to eliminate potential alteration phases like carbonates. All reported uncertainties are at the 2 σ confidence level. Isotopic ratios were determined by thermal ionization mass spectrometry (TIMS) at GEOMAR Helmholtz Centre (Kiel, Germany), utilizing a Thermo Fisher Scientific (Bremen, Germany) TRITON+ instrument for Sr and Nd measurements. The recorded $^{87}\text{Sr}/^{86}\text{Sr}$ value for the NBS987 reference material was 0.710264 ± 0.000009 [two standard deviations (2SD); n = 102], while the $^{143}\text{Nd}/^{144}\text{Nd}$ value for the La Jolla reference material was 0.511843 ± 0.000006 (2SD; n = 114). Sample data are reported relative to $^{87}\text{Sr}/^{86}\text{Sr} = 0.710250$ for NBS987 and $^{143}\text{Nd}/^{144}\text{Nd} = 0.511850$ for La Jolla. Pb isotopic ratios were determined using a TRITON+ and Finnigan MAT 262-RPQ2+. The Pb double-spike technique by [36] was applied for mass bias correction. Double-spike-corrected NBS981 values are indicated in [28] for both the TRITON+ and the MAT262 instruments. These NBS981 ratios overlap within 2SD for each instrument and align well with published double-spike and triple-spike data for NBS981 (see [36]). Chemistry blanks were monitored for each sample batch, and the amounts of Sr, Nd, and Pb were typically <100 pg (i.e., negligible compared to the sample amount).

Additionally, one extra sample underwent Sr-Nd isotope analysis by TIMS at the Laboratoire Magmas and Volcans isotope laboratory (Clermont-Ferrand, France) using a Thermo Fisher Triton instrument. Isotopic ratios of Sr and Nd were corrected for mass fractionation by normalization to $^{86}\text{Sr}/^{88}\text{Sr} = 0.1194$ and $^{146}\text{Nd}/^{144}\text{Nd} = 0.7219$, respectively. The Sr-Nd sample decomposition and chemical separation followed the procedure outlined by [37]. International standards such as NBS987 and JNd-1 yielded $^{87}\text{Sr}/^{86}\text{Sr}$ and $^{143}\text{Nd}/^{144}\text{Nd}$ values of 0.710241 ± 6 (2SD) and 0.512102 ± 4 , respectively, during the analysis period. These values fall within the accepted standard values' error range.

4. Results

4.1. Geology and Stratigraphy

Santa Clara Island is part of a large, partially eroded volcanic structure that also hosts the neighboring Robinson Crusoe Island. The smaller Santa Clara displays the same three main geological units observed on the complex [23]: (1) Punta Larga Basalts, which consists of altered basalt rocks intensely intruded by dikes; (2) Puerto Inglés Sequence, which is composed of basalt and picrite lava flows with brecciated levels and to a lesser extent intercalations of tuffs, conglomerates, and volcanic sedimentary breccias; and (3) Santa Clara Volcanoes, sequences of basanites with conglomerates and pyroclastic beds [23] (Figure 2). The first two units represent the construction of the shield volcanoes (shield stage, hereafter referred also as shield lavas), while Santa Clara Volcanoes were formed by rejuvenated magmatism after a period of ca. 2.15 My (considering that the youngest reported age of the shield stage on Robinson Crusoe is ~3.4 Ma) of volcanic quiescence [8,9,23], reflected in the conspicuous erosional unconformity that separates both. Based on new field data, it is possible to divide the Santa Clara Volcanoes unit into two sequences formed from different emission centers. In this work, these sequences will be referred to as Bahía W Sequence (BW) and Morro Spartan Sequence (MS) based on the geographical names of the locations where these sequences were described (Figure 2).

The BW is a thick volcanic sequence formed by approximately 10 lava flows with brecciated layers and intercalations of sedimentary and strongly oxidized pyroclastic deposits. The BW overlies a marked erosional unconformity that separates it from the shield lavas, suggesting its formation as the infill of a paleo-valley. From bottom to top, the sequence begins with a lava flow interbedded between conglomerates, among which a second lenticular lava flow with little lateral expression crops out. After these levels, a section with A'a-type lava flows is recognized, separated by laterally continuous layers of

strongly oxidized scoria (Figure 3). Three $^{40}\text{Ar}/^{39}\text{Ar}$ ages are available for BW [8,23], with values of 1.25 ± 0.03 Ma, 1.17 ± 0.04 Ma, and 0.90 ± 0.03 Ma (Figures 2 and 3).

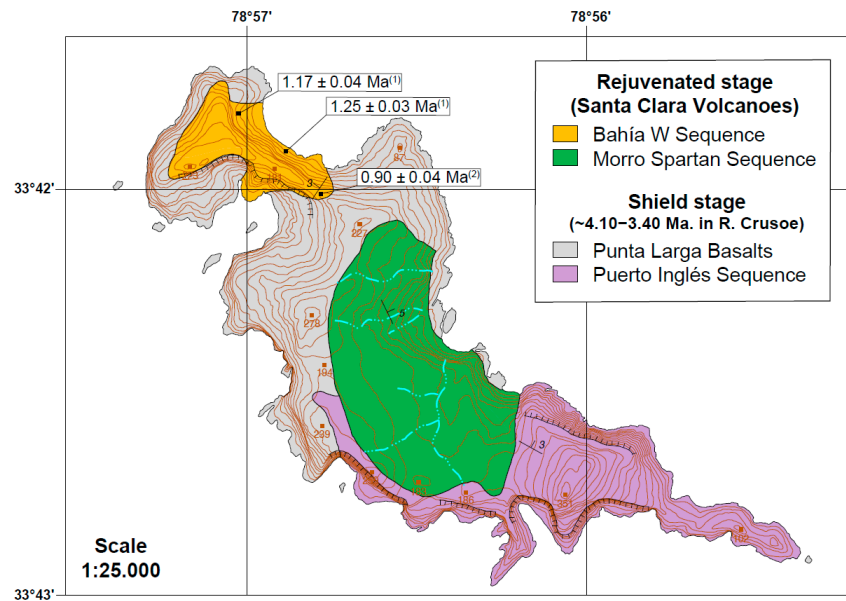


Figure 2. Geological map of Santa Clara Island modified from [23] with the geological units mentioned in the text: Punta Larga Basalts, Puerto Inglés Sequence (both representative of the shield stage), and Santa Clara Volcanoes (rejuvenated volcanism) separated into Bahía W Sequence and Santa Clara Sequence. Some dip/strike data, contour lines, and radiometric ages of the rejuvenated volcanism [8,23] are shown.

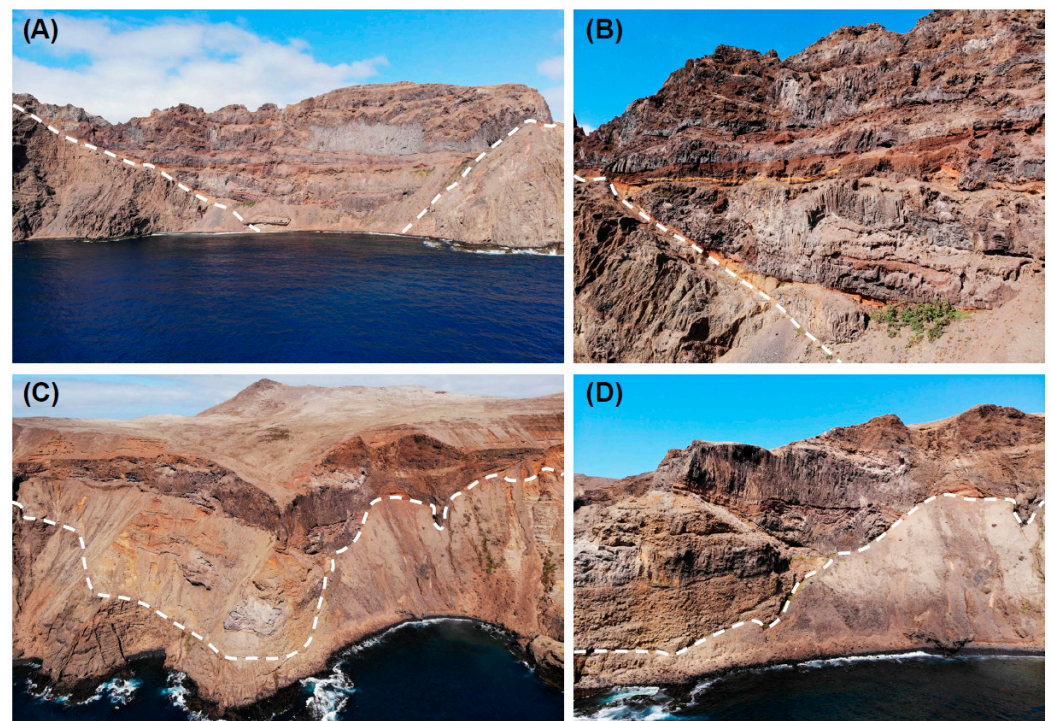


Figure 3. Aerial photographs captured by a drone of Santa Clara Island. (A) Erosional unconformity between BW and shield stage lavas suggests its formation as the infill of a paleo-valley. (B) Representative section of BW, lava flows with brecciated lavas and intercalations of sedimentary and pyroclastic deposits. (C) Erosional unconformity between MS and shield stage lavas. (D) Representative section of MS, several lava flows with local development of columnar joints over fluvial–alluvial conglomerates.

The MS is a volcanic sequence formed by 5 lava flows and a thick layer of bombs and pyroclastic deposits underlying the uppermost lava flow. The MS overlies the shield lavas through an erosional unconformity and begins with a lenticular level with columnar joints emplaced between fluvial–alluvial conglomerates. Above, various lava flows with the development of columnar joints appear, and some directly overlie the unconformity that separates MS from the shield lavas. These lava flows are interbedded with intensely oxidized scoria layers and lapilli tuffs, potentially representing remnants of an ancient volcanic structure (Figure 3). No radiometric ages have been reported for this unit. It might have lateral continuity in a small pyroclastic sequence with an intercalated lava flow that crops out towards the west.

4.2. Petrography and Mineral Chemistry

Lavas from the BW unit exhibit porphyritic textures and are composed of phenocrysts (diameter > 0.2 mm) of olivine (4.7–1.4 vol%, vesicle-free percentages; the ranges include all samples, so the maximum values do not necessarily correspond to the same sample) and clinopyroxene (6.6–0.3 vol%) with zoning and spongy texture in some crystals, embedded in a typically intersertal groundmass (91.0–81.7 vol%) which is composed of volcanic glass, olivine, clinopyroxene, Fe-Ti oxides, and plagioclase in varying proportions (Figure 4A). The presence of ultramafic xenoliths is notable (Figure 4B), reaching up to 8.9 vol% of the rock, a percentage that increases to 15.5 vol% when considering several olivine crystals that, based on their appearance and resorption rims, seem to correspond to xenocrysts. Some basalt xenoliths with sinuous rims are also observed (Figure 4C). The vesicle content (prior to normalization) is less than 5 vol%, and alteration is slight, with the scarce presence of iddingsite at olivine rims and smectite with Fe-Ti oxides in the groundmass.

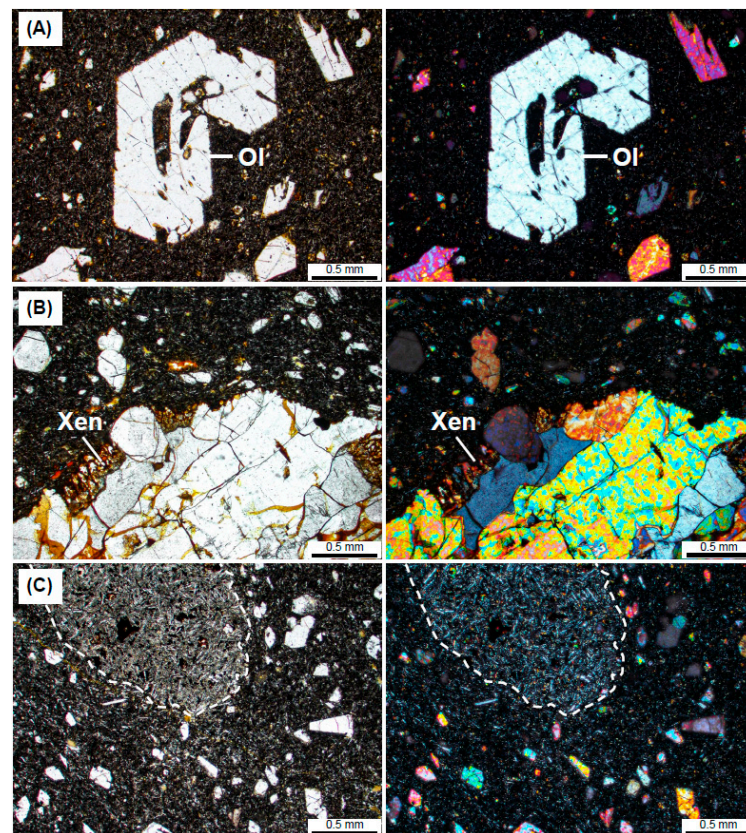


Figure 4. Representative microphotographs of volcanic rocks from rejuvenated volcanism in the BW (parallel nicols on the left and crossed nicols on the right). (A) Basanite with olivine phenocrysts with resorption rims. (B) Ultramafic xenolith with resorption. (C) Basaltic volcanic xenolith with partial resorption.

In turn, lavas from the MS unit have a porphyritic texture with olivine (8.7–2.7 vol%, vesicle-free percentages), some with resorption rims, and clinopyroxene phenocrysts (7.5–0.1 vol%) with locally spongy texture embedded in an intersertal groundmass (95.2–79.3 vol%) composed by the volcanic glass, olivine, clinopyroxene, Fe-Ti oxides, and sparsely plagioclase (Figure 5A). Towards the top of the sequence, vesicle content increases significantly, reaching up to 65.3 vol% (<5 vol% in the rest of the MS, both values prior to normalization) in uppermost samples (Figure 5B). The content of ultramafic xenoliths is significantly lower in MS compared to BW, reaching up to 1.7 vol%, increasing to 7.8 vol% when considering possible olivine xenocrysts. Again, fragments of basic volcanic rocks with sinuous margins are observed as xenoliths (Figure 5C). The rocks are slightly altered, with the presence of iddingsite rims in olivine and amygdales filled with carbonate minerals.

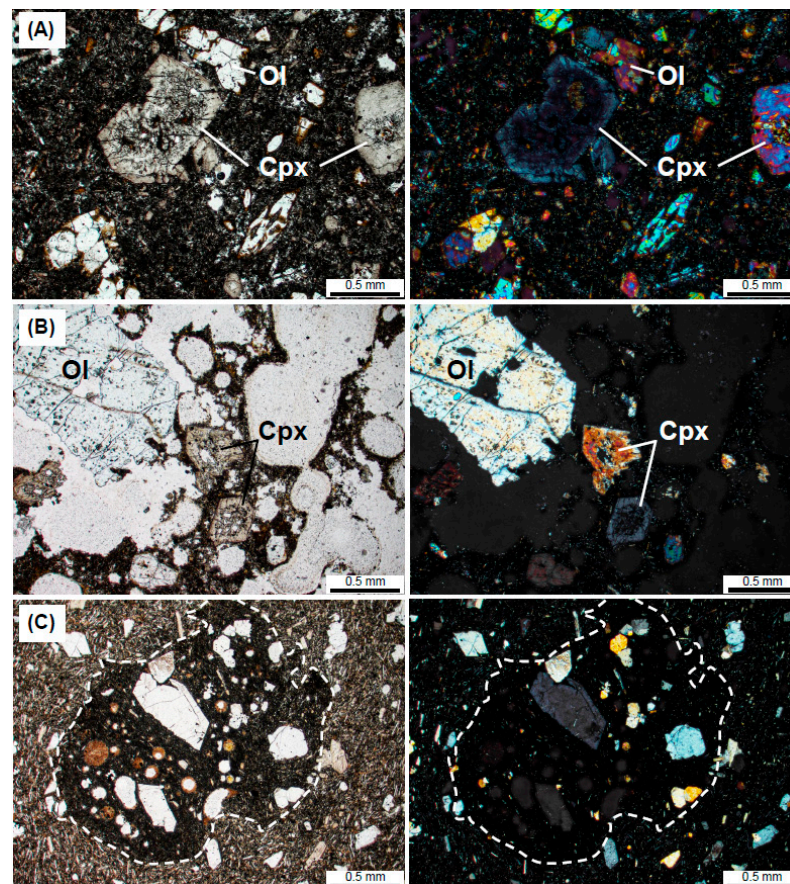


Figure 5. Representative microphotographs of volcanic rocks from rejuvenated volcanism in the MS (parallel nicols on the left and crossed nicols on the right). (A) Basanite with clinopyroxene phenocrysts showing spongy texture and olivine with resorption rims. (B) Vesicular basanite located towards the top of the MS. (C) Basaltic volcanic xenolith with partial resorption.

Based on the single sample with mineral chemistry data (part of the BW) [8], it is determined that olivine usually presents normal zoning, with more primitive cores in the $Fo_{89.7}$ – $Fo_{85.8}$ range, surrounded by thin rims in the $Fo_{82.5}$ – $Fo_{80.1}$ range (Table 2). The cores also show relative enrichments in SiO_2 , Cr_2O_3 , and NiO , and depletion in MnO and CaO , with no clear trends for TiO_2 and Al_2O_3 . Despite the high Fo values, the CaO content (0.34–0.21 wt%) (Table 2) of the analyzed cores rules out their mantle origin [38], although, based on the abundance of ultramafic xenoliths in the BW and the description for other rejuvenated lavas in JFR [8], it is possible that other crystals with a similar Fo content, without chemical data available, might be of mantle origin. The estimated temperature by [8] based on the olivine–liquid thermometer of [39] (modified from [40]) is 1270–1269 °C

(± 31 °C). In turn, clinopyroxene presents complex zoning, with compositions classified as diopside, with few exceptions plotting over the 50% wollastonite component, but are also considered as diopside for the purposes of this study (Figure 6). The crystals develop a compositional trend with higher Na₂O, MnO, and Cr₂O₃ contents in the cores (less evident for SiO₂ and MgO) compared to the rims but lower CaO (less evident for FeO^T and TiO₂). Al₂O₃ does not show a trend that allows notable differences between cores and rims. Pressures at different measured points are highly variable, with values using the barometer of [41] ranging between 8.2 and 1.1 kbar (the error of the method is ± 1.7 kbar) (this study incorporates some analyses that were not considered in the previous studies) (Table 3), with large variations even within the same crystal (8.2 to 1.8 kbar) (Figure 6). This, beyond the errors of the method, implies polybaric formation conditions for the same crystal. Additionally, two anomalous cores are recognized, very depleted in MgO and enriched in FeO^T and Na₂O with an unknown origin [8] (Table 3). No pressure estimates were made for these points, as they do not satisfy the Mg# > 0.7 condition required by the method [41].

Table 2. EPMA data (wt%) for olivine phenocrysts from the rejuvenated volcanism on Santa Clara Island (c: core, r: rim) (sample JR160913-2 from BW). Olivine–liquid temperature from [39] (± 31 °C) is also provided for the liquid–crystal equilibrium pairs. Spots marked with (*) were previously published in [8].

Spot		SiO ₂	FeO ^T	MgO	MnO	CaO	NiO	Sum	Fo	OI-Liq
Det. Limit		0.02	0.02	0.01	0.02	0.01	0.02			T (°C)
C1-O11 (*)	c	39.16	13.64	46.08	0.19	0.23	0.23	99.53	85.8	-
C1-O12 (*)	r	38.92	17.27	43.79	0.37	0.27	0.13	100.75	81.9	-
C4-O13 (*)	c	39.42	13.1	46.93	0.27	0.25	0.2	100.15	86.5	-
C4-O14 (*)	r	38.53	18.69	42.13	0.38	0.34	0.05	100.12	80.1	-
C4-O15 (*)	r	38.64	16.87	43.74	0.28	0.28	0.16	99.97	82.2	1270
C6-O16 (*)	c	39.9	10.24	49.03	0.14	0.25	0.24	99.79	89.5	-
C6-O17 (*)	c	39.57	11.13	48.44	0.15	0.23	0.29	99.8	88.6	-
C6-O18 (*)	r	38.53	18.24	42.96	0.35	0.29	0.05	100.43	80.8	-
C7-O110 (*)	c	39.82	10.01	49.14	0.19	0.21	0.33	99.7	89.7	-
C7-O111 (*)	r	38.27	17.69	43.15	0.33	0.32	0.1	99.85	81.3	-
C7-O112 (*)	c	39.98	10.12	48.7	0.18	0.21	0.29	99.49	89.6	-
C7-O113 (*)	r	38.57	16.79	43.64	0.3	0.23	0.12	99.64	82.2	1270
C8-O114 (*)	c	39.78	10.1	48.97	0.12	0.23	0.31	99.5	89.6	-
C8-O115 (*)	r	38.52	16.58	43.72	0.33	0.26	0.13	99.54	82.5	1269
C8-O116	r	38.99	16.83	44.22	0.32	0.21	0.19	100.74	82.4	1269

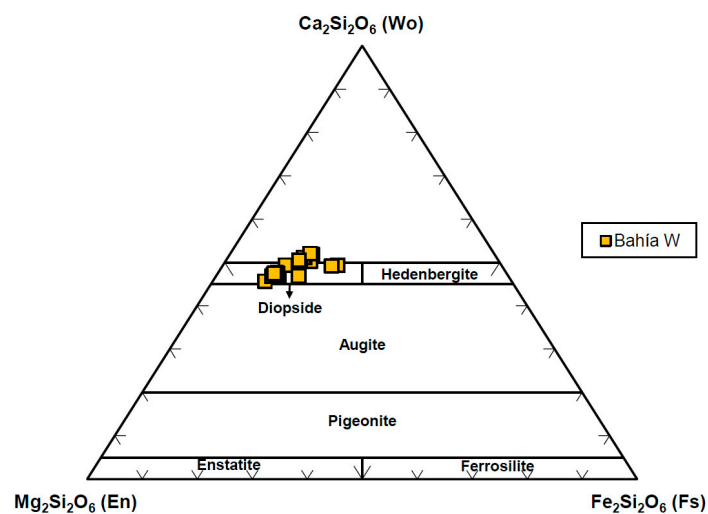


Figure 6. Classification diagram of clinopyroxene according to [42] for crystals analyzed with EPMA in a sample from the rejuvenated volcanism on Santa Clara Island.

Table 3. EPMA data (wt%) for clinopyroxene phenocrysts from the rejuvenated volcanism on Santa Clara Island (sample JR160913-2 from BW). The indicated pressure corresponds to the estimation using the barometer of [41] (± 1.7 kbar + ca. 1 kbar per 1 wt% H₂O in the melt). The two anomalous core compositions are marked with (+) (see text for details). Spots marked with (*) were published in [8].

Spot	SiO ₂	TiO ₂	Al ₂ O ₃	FeO ^T	MgO	MnO	CaO	Na ₂ O	Cr ₂ O ₃	Sum	P (kbar)
Det. Limit	0.02	0.03	0.01	0.02	0.01	0.02	0.01	0.01	0.02		
C1-Cpx1 (*)	47.56	2.15	9.29	8.40	11.98	0.13	20.50	1.06	0.00	101.07	8.0
C1-Cpx2 (*)	51.20	1.13	5.31	5.70	15.09	0.12	21.40	0.57	0.51	101.03	4.2
C1-Cpx3	41.73	4.79	11.69	8.49	10.42	0.12	22.73	0.54	0.04	100.55	2.9
C2-Cpx4 (*)	49.15	1.61	7.75	6.57	13.61	0.19	21.38	0.77	0.04	101.06	6.5
C2-Cpx5 (+)	46.66	2.19	8.89	11.19	8.94	0.35	20.63	1.70	0.00	100.54	-
C2-Cpx6	44.39	3.17	11.71	8.41	10.48	0.20	21.35	0.92	0.00	100.63	8.2
C2-Cpx7 (*)	49.09	1.52	7.89	5.93	13.83	0.14	21.35	0.78	0.69	101.23	7.2
C2-Cpx8 (*)	46.72	2.42	8.32	6.51	12.60	0.16	22.06	0.61	0.60	100.00	4.5
C2-Cpx9	43.45	4.04	9.84	7.95	11.12	0.10	22.69	0.50	0.02	99.69	1.8
C3-Cpx10 (*)	49.12	1.54	7.44	6.31	13.54	0.17	21.52	0.75	0.01	100.41	6.1
C3-Cpx11 (+)	46.75	2.45	9.41	10.64	9.32	0.29	20.63	1.52	0.00	101.02	-
C3-Cpx12 (*)	49.22	1.45	7.98	5.99	13.79	0.13	20.96	0.84	0.76	101.13	8.0
C3-Cpx13	44.23	3.95	10.00	7.88	11.28	0.12	22.91	0.49	0.03	100.86	2.3
C4-Cpx14	44.01	3.70	10.46	7.61	11.36	0.14	22.23	0.58	0.31	100.41	4.4
C4-Cpx15 (*)	50.00	1.69	5.20	6.46	14.11	0.09	22.40	0.48	0.16	100.58	1.1
C7-Cpx16 (*)	49.39	1.58	6.91	5.94	14.05	0.14	21.31	0.69	0.60	100.61	5.6
C7-Cpx17	43.05	4.78	11.16	8.20	10.56	0.12	22.92	0.58	0.00	101.37	2.7
C8-Cpx18 (*)	48.25	1.51	7.67	5.85	13.50	0.11	21.15	0.86	0.73	99.64	7.1
C8-Cpx19	44.38	3.43	10.46	7.45	11.38	0.13	22.13	0.61	0.33	100.29	5.1

4.3. Whole-Rock Geochemistry

The generally low LOI values and limited petrographic evidence of alteration allow the use of the TAS classification diagram and further analysis, and petrogenetic interpretation of the reported data. Note that Table 1 presents the measured values of all major and trace elements, while the data reported for major elements in the text and figures have been recalculated to a total of 100% on an LOI-free basis. The lava samples from the rejuvenated volcanism in Santa Clara Island have a variable SiO₂ content between 44.29 and 40.29 wt%, while the range for MgO is 13.65–8.85 wt%. According to the TAS diagram, unlike the shield lavas, all samples are alkaline, with the BW and MS lavas being exclusively classified as basanites (Figure 7). Each sequence develops different evolutionary patterns regarding MgO. In the case of the BW, negative trends are observed (i.e., an increase in concentration as MgO decreases) for Al₂O₃, Fe₂O₃^T, CaO, Na₂O, TiO₂, P₂O₅, and MnO, with unclear behavior for SiO₂ and K₂O. In turn, for the MS, negative trends are observed in SiO₂, Na₂O, K₂O, P₂O₅, and MnO, positive in Al₂O₃, and Fe₂O₃^T, CaO, TiO₂, and unclear for CaO and TiO₂. The authors of [8] classified rocks from rejuvenated volcanism based on the relative MgO and Ni content into two compositional groups called ‘High-Mg’ and ‘Low-Mg’. While this classification will not be used in this work, it is worth noting that BW samples mainly classify as ‘High-Mg’ (5 samples), with two samples in the ‘Low-Mg’ group and two samples that could be classified as intermediate in a new group called ‘Medium-Mg’. The MS only presents samples in the ‘Low-Mg’ group.

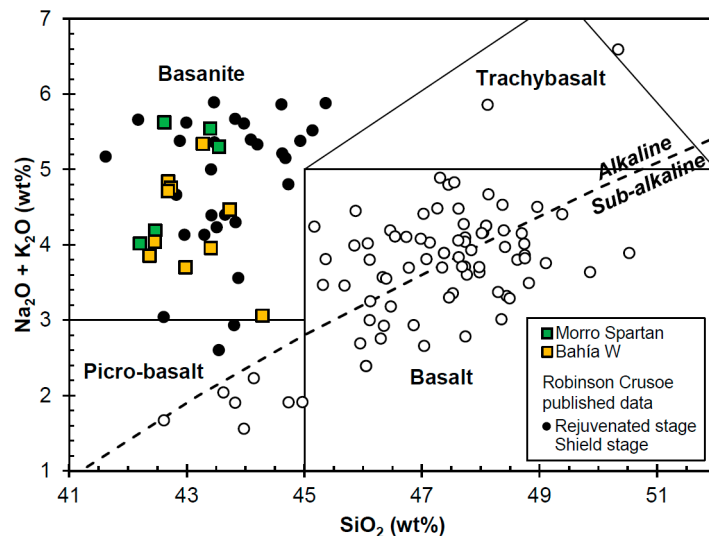


Figure 7. Total-alkali vs. silica (TAS) classification diagram for rocks from the rejuvenated volcanism on Santa Clara Island (after [43]; alkali-subalkali boundary is from [44]). Published data from the shield and rejuvenated volcanic stages of Robinson Crusoe Island are also included [8,24,28,45,46].

Trace elements show a notable geochemical enrichment of the most incompatible elements (Figure 8), reflected in high average values for the Nb/Zr and La/Yb ratios relative to shield lavas (0.26 vs. 0.16 and 22.19 vs. 12.93, respectively; shield data from [28]) and high concentrations of large-ion lithophile elements (LILE), high-field strength elements (HFSE), and light rare earth elements (LREE). The behavior of both sequences is similar, although with slightly lower values in the BW samples. Regarding internal evolutionary trends in each sequence, in the BW, an increase in Ba is observed as MgO decreases, a decrease in Ni, Cr₂O₃, Co, and V, and unclear behavior for Th, Sr, and Rb. In the MS, a negative trend of Th and positive of Ba, Sr, and Co is recognized but unclear for Ni, Cr₂O₃, Sr, and V. In both sequences, Nb, Zr, Hf, and REE increase with decreasing MgO, although a few samples deviate from the general trends. The trace element patterns on the multi-element diagram in Figure 8 are similar to the HIMU endmember from St. Helena and Mangaia (e.g., [47]).

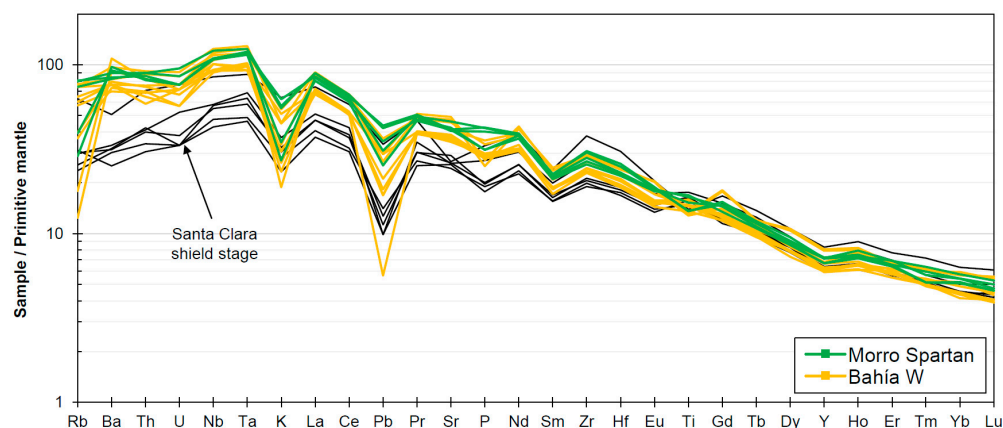


Figure 8. Primitive mantle-normalized (PM from [48]) patterns for the trace-element contents of lavas from the rejuvenated volcanism (and from the shield stage [28] for comparisons) on Santa Clara Island.

4.4. Radiogenic Isotopes

The young age of rejuvenated volcanism in Santa Clara does not require age correction of radiogenic Sr-Nd-Pb isotope data, and thus, the measured values are representative

of the magma from which the lavas originate. Three samples from the BW group were measured for Sr, Nd, and Pb isotope ratios, while a single sample from the MS was analyzed for Sr-Nd isotopic compositions. The isotopic ratios in Santa Clara are confined to $^{87}\text{Sr}/^{86}\text{Sr} = 0.70341\text{--}0.70351$, $^{143}\text{Nd}/^{144}\text{Nd} = 0.51285\text{--}0.51287$, $^{206}\text{Pb}/^{204}\text{Pb} = 19.14\text{--}19.22$, $^{207}\text{Pb}/^{204}\text{Pb} = 15.59$, and $^{208}\text{Pb}/^{204}\text{Pb} = 39.10$ to 39.16 (Table 4). In Sr-Nd isotope space, the data are negatively correlated and broadly align in the vicinity of FOZO [34], overlapping with the depleted end of the JFR shield lava array and could reflect the mixture between a depleted (DM or HIMU) and an enriched component (EM1 in this case, for the shield stage the role of EM2 seems to be more significant) with a relatively higher contribution of the latter in the MS group (Figure 9) (representative isotopic ratios of DM, HIMU, EM1, and EM2 were taken from [31]). The uraniumogenic Pb isotope diagram shows a slightly less radiogenic trend (compared to shield lavas) for $^{207}\text{Pb}/^{204}\text{Pb}$ at a given $^{206}\text{Pb}/^{204}\text{Pb}$; the latter ratio shows no distinguishable differences. The internal variation and trend of the data suggest the involvement of EM1 and HIMU components (Figure 9), which helps clarify what is indicated by the Sr vs. Nd diagram, as there does not seem to be a major or noticeable influence from DM or EM2. The thorogenic Pb isotope diagram shows the presence of the DUPAL anomaly typical of the Southern Hemisphere [49]. However, in contrast to previous systems, it is remarkable that the isotopic ratios of $^{208}\text{Pb}/^{204}\text{Pb}$ for a given $^{206}\text{Pb}/^{204}\text{Pb}$ are above the EM1 (or DM)—HIMU trend of the shield lavas (Figure 9). This could indicate the involvement of EM2, suggesting that the isotopic signature of rejuvenated volcanism in Santa Clara does not fit into traditional oceanic mantle mixing schemes. Nonetheless, the data correlation is predominantly subparallel to the trend between EM1 and HIMU, implying that these mantle components are mainly involved in the formation of the rejuvenated lavas. The trace element characteristics of the rejuvenated lavas suggest that the HIMU endmember is the major component in the rejuvenated stage lavas.

Table 4. Isotopic ratios of Sr, Nd, and Pb for samples from the rejuvenated volcanism on Santa Clara Island. Standard error (2σ) and laboratory of analysis are indicated (a: GEOMAR Helmholtz Centre, Kiel, Germany; b: Laboratoire Magmas and Volcans, Clermont-Ferrand, France).

Sample	$^{87}\text{Sr}/^{86}\text{Sr}$	\pm	$^{143}\text{Nd}/^{144}\text{Nd}$	\pm	$^{206}\text{Pb}/^{204}\text{Pb}$	\pm	$^{207}\text{Pb}/^{204}\text{Pb}$	\pm	$^{208}\text{Pb}/^{204}\text{Pb}$	\pm	Lab
Bahía W											
LL230112-4	0.703469	5	0.512868	3	19.1394	6	15.5902	5	39.1037	16	(a)
JR230112-1	0.703408	5	0.512869	4	19.2205	7	15.5939	9	39.1550	29	(a)
JR160913-2	0.703466	5	0.512861	4	19.1866	14	15.5893	12	39.1392	34	(a)
Morro Spartan											
JR230112-3	0.703508	6	0.512851	6	-	-	-	-	-	-	(b)

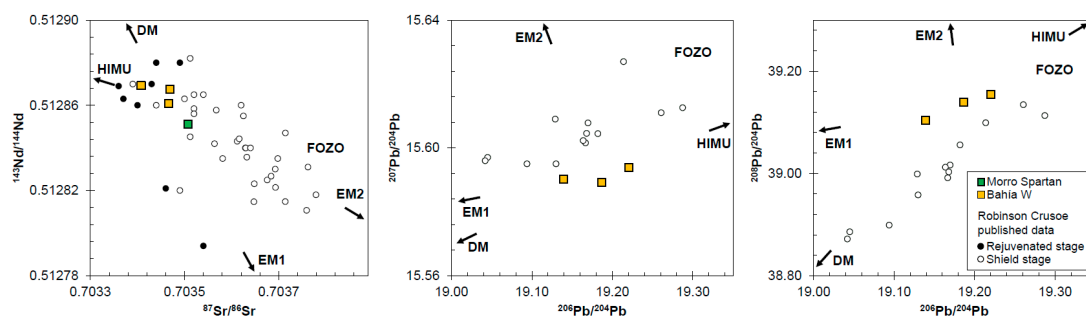


Figure 9. Diagrams showing the isotopic variations ($^{87}\text{Sr}/^{86}\text{Sr}$ vs. $^{143}\text{Nd}/^{144}\text{Nd}$; $^{206}\text{Pb}/^{204}\text{Pb}$ vs. $^{207}\text{Pb}/^{204}\text{Pb}$ and $^{206}\text{Pb}/^{204}\text{Pb}$ vs. $^{208}\text{Pb}/^{204}\text{Pb}$) in samples from the rejuvenated volcanism on Santa Clara Island. Previous data from Robinson Crusoe Island are also included [26,28,45,46]. The Pb data from [26] are not shown due to analytical complications, likely due to within-run fractionation and/or problems with Pb-double-spike application and deconvolution (see [28] for details). Representative isotopic ratios of DM, HIMU, EM1, and EM2 were taken from [31], and those of FOZO are close to the most enriched values within the ranges proposed by [34].

5. Discussion

5.1. Magmatic Evolution of the Rejuvenated Volcanism in Santa Clara

The compositional variation in the rejuvenated volcanism in Santa Clara can be explained by differentiation processes that slightly modified the original magma chemistry. For the BW, a group of samples with high MgO and Ni content is observed, coinciding with a notable presence of ultramafic xenoliths and olivine xenocrysts. The accumulation of such ultrabasic compositions would alter the geochemistry of this group and overprint primary magmatic liquids despite the careful avoidance of including ultramafic fragments in the analyzed powders. In turn, fractional crystallization of olivine would control the evolutionary trend observed for lavas of the BW (not as clear in the MS) (Figure 10). Additionally, the variation observed for CaO vs. Sc indicates that clinopyroxene fractionation also contributes to the magmatic evolution of the BW and MS (Figure 10).

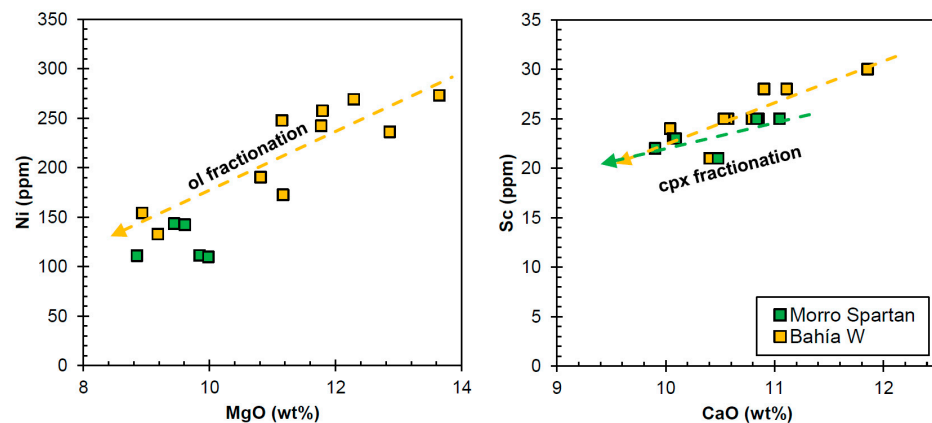


Figure 10. MgO (wt%) vs. Ni (ppm) and CaO (wt%) vs. Sc (ppm) diagrams for samples from the rejuvenated volcanism on Santa Clara Island. Dotted lines show internal evolutionary trends for BW and MS, interpreted as representative of olivine and clinopyroxene fractionation.

To confirm the involvement of olivine and clinopyroxene fractionation in the magmatic evolution of the BW and MS, thermodynamic modeling was performed using the alphaMELTS 1.9 software (version MELTS) [50–52]. Isobaric and polybaric conditions were considered, aligning with the ascent and storage models proposed for rejuvenated volcanism on Robinson Crusoe Island [8], with an oxygen buffer of QFM recommended for OIB-type compositions [53]. According to [54], based on trace element geochemistry, the water content of shield lavas was considered to be approximately 0.8 wt%. Therefore, three possible water contents were considered in our models: 1.6, 0.8, and 0.0 wt%, corresponding to double, the same, or no water compared to shield lavas. To determine the pressure to be used in the models, estimated ranges of 11–9 kbar for clinopyroxene from ultramafic xenoliths [8] and 8.2–1.1 kbar for a basanite from BW are considered. Hence, models are evaluated at 10 kbar and 2 kbar for isobaric conditions (with the three different H₂O contents in each case) and from 10 to 0 kbar at dP/dT of 50 bar/°C for polybaric conditions (H₂O content of 1.6 wt%), considered plausible values for this magmatic system. It is thought that any pressure value within these ranges will yield intermediate results for the liquid lines of descent. In fact, the models can emulate the evolutionary trends of most elements (Figure 11) through olivine and clinopyroxene (\pm spinel \pm whitlockite) fractionation at high pressure from a primitive liquid. For example, satisfactory conditions are considered at 10 kbar and H₂O of 0.0 wt%, with a liquid line of descent also generated by increasing both H₂O content and pressure, for instance, at 0.8 wt% H₂O and 13 kbar or at 1.6 wt% H₂O and 16 kbar (Figure 11). As the behavior of MgO does not always form clear trends in the samples from Santa Clara (especially in the BW), there is a possibility that it has been mobilized in some samples or its concentration is affected by the presence of xenoliths, so Fe₂O₃^T is also considered as an index of differentiation. The results of the Fe₂O₃^T vs. trace element models confirm that the aforementioned conditions are the ones

that best satisfy the observed compositional evolution in Santa Clara (Figure 11), except for some samples from BW, likely influenced by the presence of xenoliths, mobilization, or with compositional variations attributable to the source. Fractionation at pressures lower than those mentioned, under both isobaric and polybaric conditions, is ruled out, necessitating the existence of high-pressure crystallization events as a primary control of the observed chemical variations, which apparently were not recorded in the crystals analyzed by [8]. Following this, the magmas would experience polybaric crystallization from ~11 kbar (likely without substantial fractionation) with relatively direct ascent in some cases, while in others, they experienced short-lived stays in transient reservoirs that allowed the preservation of the observed zoning in olivine [8].

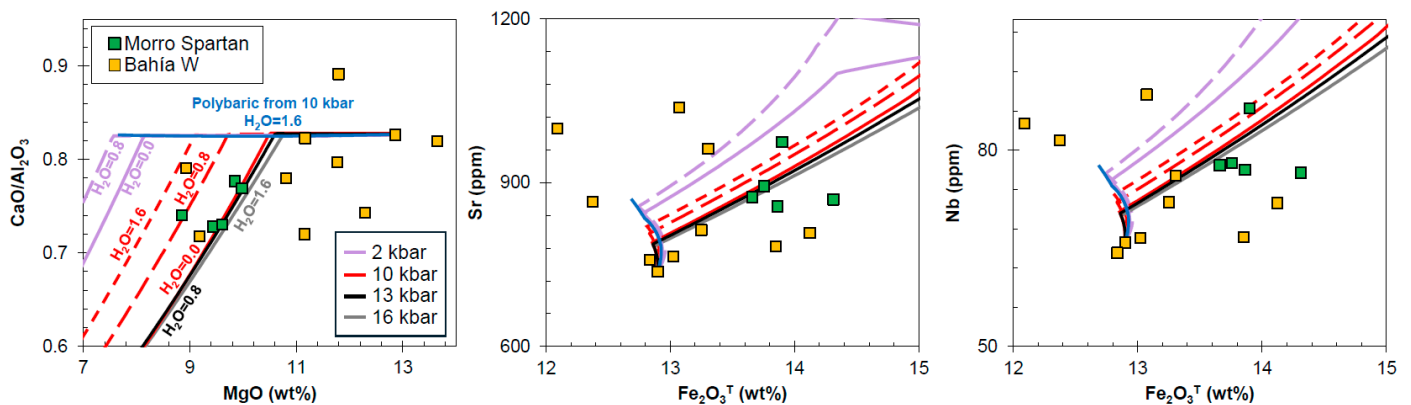


Figure 11. MgO (wt%) vs. CaO/Al₂O₃, Fe₂O₃^T (wt%) vs. Sr (ppm), and Nb (ppm) diagrams for lavas from the rejuvenated volcanism on Santa Clara Island showing the results of the fractional crystallization model performed in AlphaMELTS 1.9 software [50–52]. The input variables for each model (isobaric and polybaric with different water contents) are shown in the first graph and are the same for the following two. Fractionation at 10 kbar in an anhydrous system, or at higher pressures if the water content is higher, approximately an increase of 3 kbar for every increment of 0.8 wt% of H₂O (e.g., 13 kbar with 0.8 wt% of water, or 16 kbar with 1.6 wt%), were considered appropriate for explaining the magmatic evolution (except for some samples from the BW, likely affected by other processes).

However, for some elements, such as LILE and SiO₂, the liquid line of descent of the model does not fully satisfy the evolutionary path for both BW and MS, showing a slight trend towards less enriched compositions. This could be interpreted as a subtle mobilization of these elements or as the effect of some other process involved in differentiation that could be studied with greater availability of data. Regardless of the specific conditions of water and pressure, it is confirmed that high-pressure fractionation is the main process involved in the magmatic evolution of the rejuvenated volcanism in Santa Clara.

5.2. Is the Oceanic Lithosphere the Source of the Rejuvenated Volcanism in Santa Clara?

The metasomatized oceanic lithosphere has been widely recognized as the mantle source for some cases of rejuvenated volcanism, especially when significant temporal gaps of volcanic activity have been reported after the shield stage (which implies a considerable distance from the main axis of the mantle plume that fed the shield stage). This type of source has been proposed for Samoa [7], the Selvagen [22], Canary [21] Cook-Austral [55], Fieberling-Guadalupe [56], and Hawaii [15,16]. For JFR, a depleted lithospheric mantle source was proposed for the rejuvenated lavas based on Os isotopes, polluted by the high ³He/⁴He signature from the main shield stage [27]. However, the reported ¹⁸⁷Os/¹⁸⁸Os ratios (0.134–0.122) are not entirely conclusive; in fact, they are partially within the range of Os isotope ratios reported for the shield stage of JFR originating from a mantle plume (Robinson Crusoe: 0.143–0.128 and Alejandro Selkirk: 0.138–0.126). They are also similar to those of the Samoa shield (0.132–0.128), where a plume origin was also proposed [57].

Usually, the influence of the oceanic lithosphere is associated with isotopic depletions compared to shield lavas, trending towards the depleted mantle (DM). This is because it is assumed that originally, the oceanic lithosphere had a DM-type isotopic composition, which could have been metasomatized by the passage of melts generated in the shield stage, potentially modifying the original isotopic content of the lithospheric mantle and giving it a signature between DM and the shield lavas (e.g., [16,58]). Similarly, the mantle could be affected by the metasomatism of the lithospheric mantle by previous melts generated from another mantle plume or by other intraplate volcanism. In this case, the resulting isotopic signature would fall between that of this OIB system and the DM (e.g., the influence of another plume in Samoa [7]). Finally, another potential lithospheric source is the partial melting of the mafic and ultramafic cumulates from the previous stage. In this case, due to the short time elapsed between both shield and rejuvenated stages in Santa Clara (~2.15 Ma)—practically incapable of generating enough decay to alter the isotopic ratios—this process should produce signatures similar to those of the shield lavas.

To assess the feasibility of the oceanic lithosphere being the source of rejuvenated volcanism in Santa Clara, isotopic mixing models were developed between the DM and shield lavas. Two different compositions for the DM were considered (representative of local MORB): one corresponding to the average of available data for the North Chile Rise (including the Valdivia Fracture Zone) [59] and another to the average of published data for the East Pacific Rise (taken from the GEOROC database), which are the ridges from which the Nazca Plate on which JFR is located were formed. The samples collected from the South Chile Rise and those from the Easter Microplate were excluded due to their geographical location (unrelated to the generation of the oceanic plate beneath JFR) (Figure 1) and subduction effect in the former case [59,60] and relatively enriched isotopic values due to the influence of the Easter mantle plume in the latter [61]. For shield lavas, the most isotopically enriched value reported for Robinson Crusoe Island was considered (sample MP260112-1 from [28], the sample with available isotopic data of Sr, Nd, and Pb with the lowest $^{143}\text{Nd}/^{144}\text{Nd}$ ratio), assuming these data are also representative of Santa Clara, as both islands belong to the same large volcanic complex. Due to its geographical location, it is not possible for the lithospheric mantle beneath JFR to have previously passed over the other mantle plumes in the SE Pacific associated with Easter or San Félix—San Ambrosio Islands, which are not genetically related to JFR. Therefore, it is not considered plausible that their melts have metasomatized the lithosphere beneath Santa Clara, and only the two types of DM will be considered for the model.

The models show that, while it is possible to recognize that the rejuvenated volcanism has a very similar enriched isotopic signature to the shield lavas, a slight relative isotopic depletion can be observed in some ratios. However, these values do not lie on the mixing lines or curves between DM and shield lavas but are slightly shifted, with lower values than expected for $^{87}\text{Sr}/^{86}\text{Sr}$ and $^{143}\text{Nd}/^{144}\text{Nd}$, higher for $^{208}\text{Pb}/^{204}\text{Pb}$, and notably different for $\Delta 7/4 \text{ Pb}$ and $\Delta 8/4 \text{ Pb}$ (lower and higher, respectively) (Figure 12). The latter complicates an exclusively lithospheric origin for the rejuvenated volcanism in Santa Clara and suggests an enriched source with a somewhat different composition than proposed for the shield lavas. In particular, the high isotopic ratio of $^{208}\text{Pb}/^{204}\text{Pb}$ and $\Delta 8/4 \text{ Pb}$ in the BW suggests the participation of a source even more enriched in this ratio than the plume source from which the shield lavas originated. However, it implies that the oceanic lithosphere might not be the primary source of magmatism.

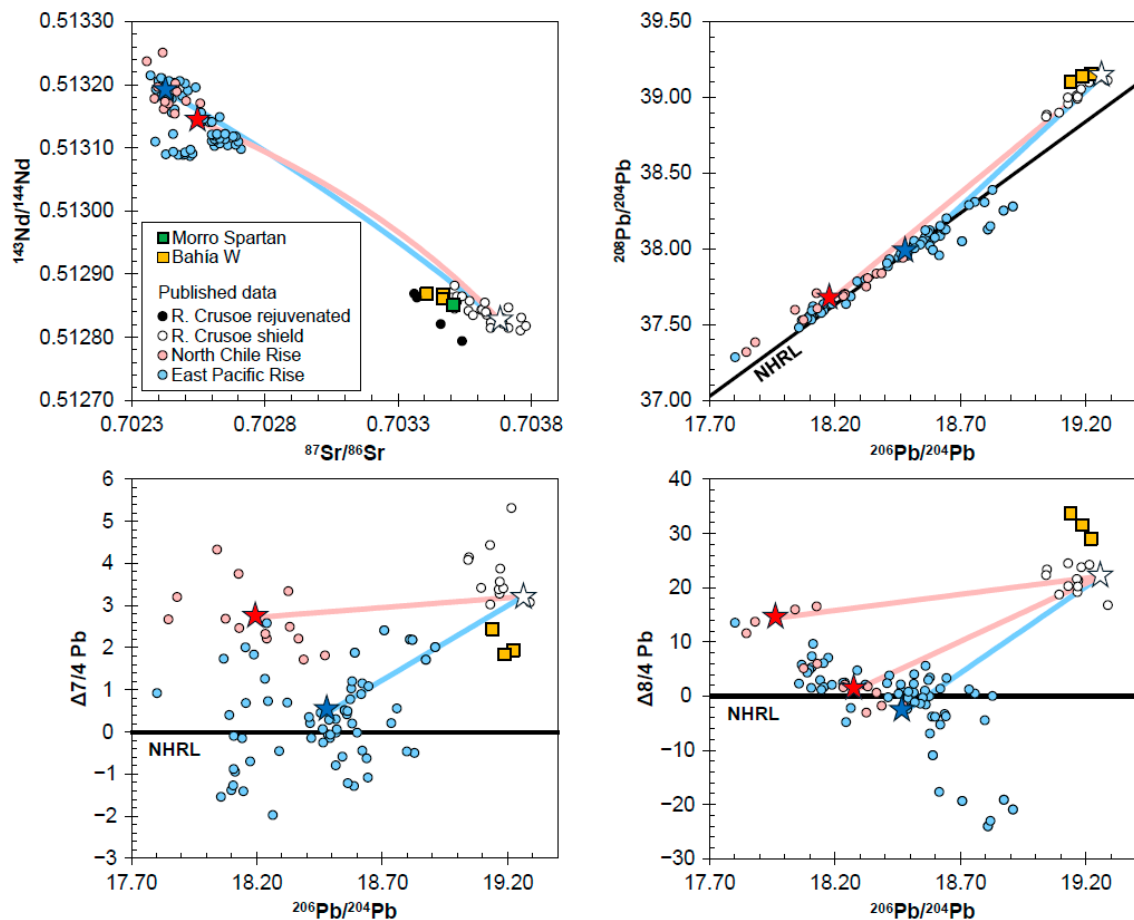


Figure 12. Isotopic ratio diagrams ($^{87}\text{Sr}/^{86}\text{Sr}$ vs. $^{143}\text{Nd}/^{144}\text{Nd}$; $^{206}\text{Pb}/^{204}\text{Pb}$ vs. $^{208}\text{Pb}/^{204}\text{Pb}$, $^{206}\text{Pb}/^{204}\text{Pb}$ vs. $\Delta 7/4 \text{ Pb}$, $^{206}\text{Pb}/^{204}\text{Pb}$ vs. $\Delta 8/4 \text{ Pb}$) showing the model that evaluates the participation of lithospheric mantle as the source of rejuvenated volcanism on Santa Clara Island. In detail, the model considers the mixing between depleted mantle (DM) represented by samples from the North Chile Rise [59] and East Pacific Rise (data taken from the GEOROC database) and the shield stage of Robinson Crusoe (assumed to be analogous to Santa Clara). For the mixing curves, the average values of the isotopic ratios of each sample set (with the average Sr-Nd content) were considered as endmembers for the DM, the red star representing North Chile Rise (with two endmembers in the last graph due to the data dispersion) and the blue star representing East Pacific Rise. Meanwhile, for the shield stage, the sample with the lowest $^{143}\text{Nd}/^{144}\text{Nd}$ ratio (considering only samples with available Pb isotopes) was chosen as representative of the more enriched source (white star). NHRL: North Hemisphere Reference Line [49].

5.3. Is a Mantle Plume the Source of the Rejuvenated Volcanism in Santa Clara?

An alternative previously proposed for various cases like Hawaii [13,14], Marquesas [62,63], Mauritius [17], and Canary [18,20,21] is that the source of rejuvenated volcanism is a mantle plume—the same one that previously melted to feed the magmatism of the shield stage or from a separate plume that the lithosphere moves over after the first phase of volcanism, as observed in Walvis [64]. In Santa Clara, the geochemistry of the rejuvenated volcanism is enriched compared to the shield lavas, yet the heavy rare earth elements (Figure 8) and certain ratios of incompatible elements representatives of the mantle source are very similar in both stages. For instance, the ratio of $(\text{Hf}/\text{Sm})_{\text{N}}$ vs. SiO_2 , $\text{Na}_2\text{O} + \text{K}_2\text{O}$, and CaO (wt%) (Figure 13) shows no variations that could be interpreted as changes in the degree of carbonatite fluxing [65] or remarkably distinct mantle compositions. At most, they could indicate slight variations in the depth or degree of melting [65]. This suggests

a source for the rejuvenated volcanism similar to that which generated the shield stage, characterized as a slightly heterogeneous mantle plume [24–28].

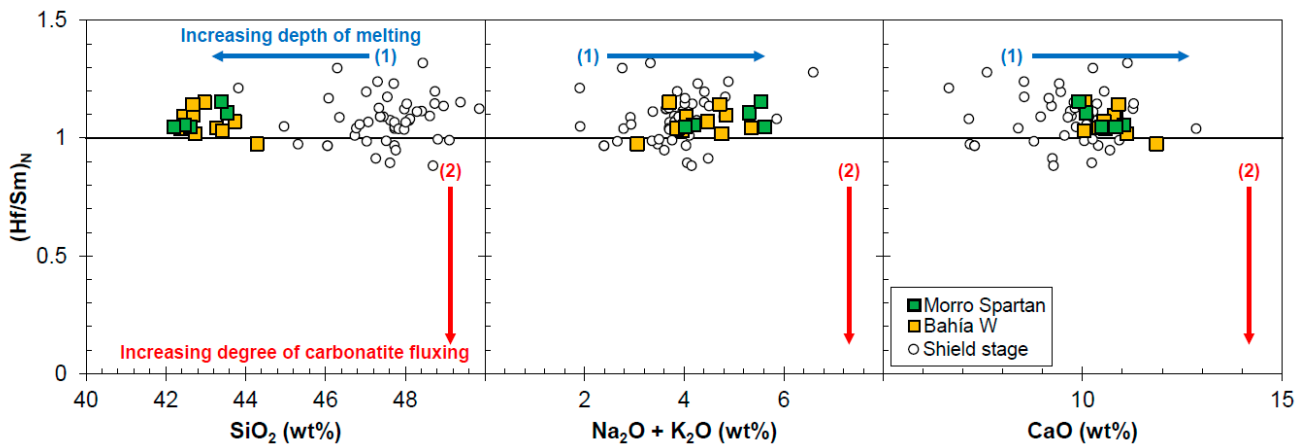


Figure 13. $(\text{Hf}/\text{Sm})_N$ vs. SiO_2 , $\text{Na}_2\text{O} + \text{K}_2\text{O}$, and CaO (wt%) diagrams for lavas from the rejuvenated volcanism on Santa Clara Island. Published values from the shield stage in Santa Clara and Robinson Crusoe are also shown for comparison [8,24,26,28]. Trends interpreted as increasing depth of melting and increasing degree of carbonate fluxing were taken from [65].

Another argument for proposing the heterogeneous mantle plume of JFR as the source of rejuvenated volcanism in Santa Clara is its isotopic signature, especially the particular values of $^{208}\text{Pb}/^{204}\text{Pb}$, the highest for a given $^{206}\text{Pb}/^{204}\text{Pb}$ reported for the Nazca Plate in the vicinity of JFR (only comparable to San Félix—San Ambrosio, which has a similar signature for Pb isotopes, but notably more enriched in Sr and Nd) (Figure 14). These values might originate from the intrinsic heterogeneity of the plume, with selective sampling of a component enriched in thorogenic lead during rejuvenated volcanism or, alternatively, a decrease in the proportion of other components sampled more extensively during the shield stage. Adding to the evidence in favor of a plume origin is that the internal trends of the data obtained for the BW are subparallel to the mixing line between EM1 and HIMU components (Figure 9). These are two mantle sources typically associated with plumes and represent the recycling of different sections of old oceanic lithosphere through subduction processes, which over time generate unique isotopic and compositional characteristics for each (e.g., [31,35,36,47,66–71]).

Since the rejuvenated stage lavas cannot be explained by mixing common upper mantle endmembers (North Chile Rise or East Pacific Rise) and the rejuvenated stage lavas show similarities to the shield stage lavas, which have high $^3\text{He}/^4\text{He}$ ratios and thus must be plume derived, the most likely origin for the rejuvenated volcanism is the plume, representing a slightly different plume flavor from the shield stage lavas. Additionally, the short time elapsed between the shield and rejuvenated volcanism in Santa Clara, at most ~ 2.15 Ma (considering the available ages for the shield stage at Robinson Crusoe Island; [23,29]), implies that the oceanic plate has moved ~ 152 km from the plume center if the mantle plume is stationary and the Nazca Plate moves 70.55 mm/yr eastward, or more precisely ~ 174 km if the hotspot drift and a moving plume is considered [29]. This would result in a distinct melting zone from the shield stage lavas formed from the center of the plume, allowing a slightly different plume flavor to be sampled. Alternatively, differences in melting conditions could result in an isotopically distinct component being melted during rejuvenated volcanism than during shield stage volcanism. The latter has been proposed for Hawaii [72] and Marquesas [73]. In conclusion, the available evidence favors the hypothesis of rejuvenated volcanism in Santa Clara being generated by the melting of the JFR mantle plume from which the shield stage lavas were also generated. The heterogeneities of this plume are represented by variable contributions of different EM1 and HIMU/FOZO type components.

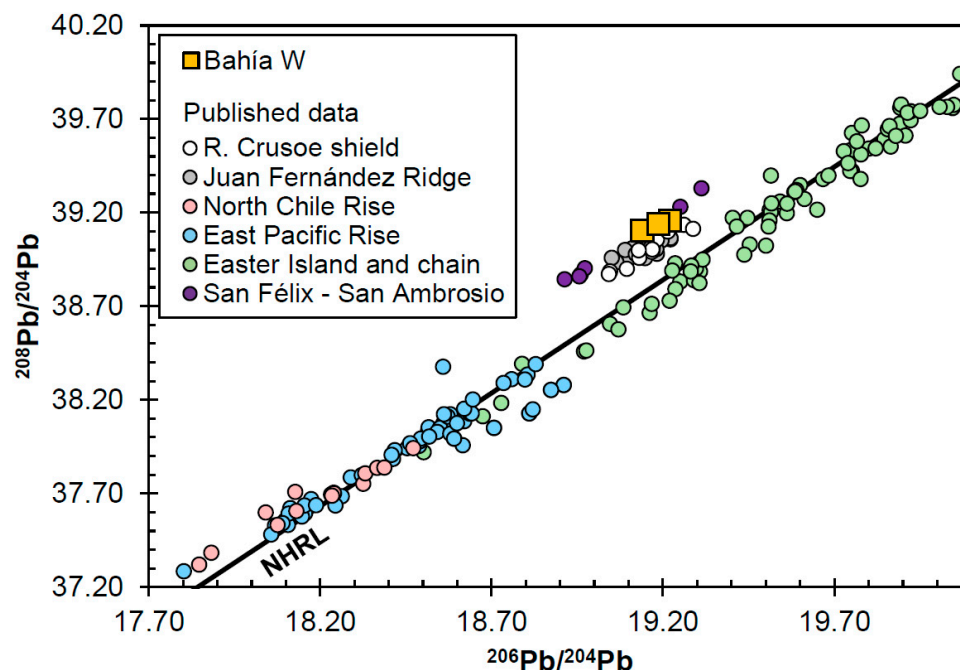


Figure 14. $^{206}\text{Pb}/^{204}\text{Pb}$ vs. $^{208}\text{Pb}/^{204}\text{Pb}$ diagram for representative samples of the rejuvenated volcanism on Santa Clara Island. Data (taken from the GEOROC database) for the Nazca Plate in the vicinity of JFR are also included: North Chile Rise, East Pacific Rise (both representative of local MORB), Easter Island and Easter seamount chain, San Félix—San Ambrosio (representative of other mantle plumes in the SE Pacific), and JFR itself. The $^{208}\text{Pb}/^{204}\text{Pb}$ values of rejuvenated volcanism on Santa Clara are the highest for a given $^{206}\text{Pb}/^{204}\text{Pb}$ among all reported data (only comparable to San Félix—San Ambrosio; see Figure 1 for their location). Data from the South Chile Rise and Easter Microplate were not included (see Section 5.2 for details).

6. Conclusions

The JFR exhibits at least two stages of volcanism with marked compositional differences. Santa Clara Island appears to have had at least two rejuvenated volcanisms, consisting of two sequences (BW and MS) formed by basanites and picrobasalts geochemically enriched compared to the shield stage. The isotopic ratios of Sr, Nd, and Pb are broadly similar to the shield lavas, but slight deviations indicative of small source differences are present. Geochemistry reveals a complex magmatic evolution, including polybaric fractional crystallization of olivine and clinopyroxene. Although there are slight differences in isotopic composition between shield and rejuvenated volcanism, depleted upper mantle similar to North Chile Rise and East Pacific Rise MORB does not appear to play an important role in the generation of either magmatic stage. The overall similarity in isotopic composition suggests that the rejuvenated volcanism is also derived from the mantle plume. This reinforces the idea of a heterogeneous plume involved in the petrogenesis of JFR volcanism. Nonetheless, further research is needed to elucidate the exact mechanisms driving the magmatic evolution and the extent of lithospheric influence.

Author Contributions: Fieldwork, J.R., L.E.L., V.S. and C.O.; Petrography and mineral chemistry, J.R., L.E.L., N.A. and C.O.; Whole-rock geochemistry, J.R., L.E.L. and C.O.; Radiogenic isotopes, J.R., V.S., F.H. and K.H.; Figures and tables, J.R. The main author conceived this study and wrote the original draft, which was later improved with input from L.E.L., V.S., N.A., C.O., F.H. and K.H. All authors have read and agreed to the published version of the manuscript.

Funding: This research was supported by the ANID FONDECYT Iniciación 11200942, Chile (PI J. Reyes) and ANID FONDECYT 1211792, Chile (PI L.E. Lara).

Data Availability Statement: Data are contained within the article.

Acknowledgments: The authors are grateful to the reviewers and editor for their contribution to improving this paper. We also want to express our gratitude to the Corporación Nacional Forestal (CONAF), Chile, and the staff of Parque Nacional Archipiélago de Juan Fernández for their valuable logistical support during the field campaigns. Finally, we thank J-L. Paquette (who passed away in 2022, may he rest in peace), D. Auclair, and C. Bosq from Clermont-Ferrand for performing one of the Sr-Nd analyses. The GEOMAR Helmholtz Centre for Ocean Research Kiel (F. Hauff and K. Hoernle) is thanked for supporting the isotopic analyses.

Conflicts of Interest: The authors declare no conflicts of interest.

References

- McDougall, I. Potassium-Argon Ages from Lavas of the Hawaiian Islands. *GSA Bull.* **1964**, *75*, 107–128. [\[CrossRef\]](#)
- McDougall, I. The geochronology and evolution of the young volcanic island of Réunion, Indian Ocean. *Geochim. Cosmochim. Acta* **1971**, *35*, 261–288. [\[CrossRef\]](#)
- Morgan, W.J. Convection plumes in the lower mantle. *Nature* **1971**, *230*, 42–43. [\[CrossRef\]](#)
- Morgan, W.J. Deep mantle convection plumes and plate motions. *Am. Assoc. Pet. Geol. Bull.* **1972**, *56*, 203–213. [\[CrossRef\]](#)
- García, M.O.; Weis, D.; Jicha, B.R.; Ito, G.; Hanano, D. Petrology and geochronology of lavas from Ka’ula Volcano: Implications for rejuvenated volcanism of the Hawaiian mantle plume. *Geochim. Cosmochim. Acta* **2016**, *185*, 278–301. [\[CrossRef\]](#)
- Wright, E.; White, W.M. The origin of Samoa: New evidence from Sr, Nd, and Pb isotopes. *Earth Planet. Sci. Lett.* **1987**, *81*, 151–162. [\[CrossRef\]](#)
- Konter, J.G.; Jackson, M.G. Large volumes of rejuvenated volcanism in Samoa: Evidence supporting a tectonic influence on late-stage volcanism. *Geochim. Geophys. Geosyst.* **2012**, *13*, Q0AM04. [\[CrossRef\]](#)
- Reyes, J.; Lara, L.E.; Morata, D. Contrasting P-T paths of shield and rejuvenated volcanism at Robinson Crusoe Island, Juan Fernández Ridge, SE Pacific. *J. Volcanol. Geotherm. Res.* **2017**, *341*, 242–254. [\[CrossRef\]](#)
- Lara, L.E.; Díaz-Naveas, J.; Reyes, J.; Jicha, B.; Orozco, G.; Tassara, A.; Kay, S. Unraveling short-lived rejuvenated volcanism and a rapid transition from shield stage at O’Higgins Guyot, Juan Fernández Ridge, Pacific SE. *Deep.-Sea Res. Part I Oceanogr. Res. Pap.* **2018**, *141*, 33–42. [\[CrossRef\]](#)
- Ozawa, A.; Tagami, T.; García, M.O. Unspiked K-Ar dating of the Honolulu rejuvenated and Ko’olau shield volcanism on O’ahu, Hawai’i. *Earth Planet. Sci. Lett.* **2005**, *232*, 1–11. [\[CrossRef\]](#)
- Clague, D.A.; Frey, F.A. Petrology and Trace Element Geochemistry of the Honolulu Volcanics, Oahu: Implications for the Oceanic Mantle below Hawaii. *J. Petrol.* **1982**, *23*, 446–504. [\[CrossRef\]](#)
- Maaløe, S.; James, D.; Smedley, P.; Petersen, S.; Garmann, L.B. The Koloa Volcanic Suite of Kauai, Hawaii. *J. Petrol.* **1992**, *33*, 761–784. [\[CrossRef\]](#)
- García, M.O.; Swinnard, L.; Weis, D.; Greene, A.R.; Tagami, T.; Sano, H.; Gandy, C.E. Petrology, geochemistry and geochronology of Kaua’i lavas over 4–5 Myr: Implications for the origin of rejuvenated volcanism and the evolution of the Hawaiian plume. *J. Petrol.* **2010**, *51*, 1507–1540. [\[CrossRef\]](#)
- Béguelin, P.; Bizimis, M.; McIntosh, E.C.; Cousens, B.; Clague, D.A. Sources vs processes: Unraveling the compositional heterogeneity of rejuvenated-type Hawaiian magmas. *Earth Planet. Sci. Lett.* **2019**, *514*, 119–129. [\[CrossRef\]](#)
- Lassiter, J.C.; Hauri, E.H.; Reiners, P.W.; García, M.O. Generation of Hawaiian post-erosional lavas by melting of a mixed lherzolite/pyroxenite source. *Earth Planet. Sci. Lett.* **2000**, *178*, 269–284. [\[CrossRef\]](#)
- Yang, H.-J.; Frey, F.A.; Clague, D.A. Constraints on the Source Components of Lavas Forming the Hawaiian North Arch and Honolulu Volcanics. *J. Petrol.* **2003**, *44*, 603–627. [\[CrossRef\]](#)
- Paul, D.; White, W.M.; Blichert-Toft, J. Geochemistry of Mauritius and the origin of rejuvenescent volcanism on oceanic island volcanoes. *Geochim. Geophys. Geosyst.* **2005**, *6*, Q06007. [\[CrossRef\]](#)
- Hoernle, K.; Tilton, G.; Schmincke, H.-U. Sr-Nd-Pb isotopic evolution of Gran Canaria: Evidence for shallow enriched mantle beneath the Canary Islands. *Earth Planet. Sci. Lett.* **1991**, *106*, 44–63. [\[CrossRef\]](#)
- Hoernle, K.; Schmincke, H.-U. The petrology of the tholeiites through melilite nephelinites on Gran Canaria, Canary Islands: Crystal fractionation, accumulation and depths of melting. *J. Petrol.* **1993**, *34*, 573–597. [\[CrossRef\]](#)
- Hoernle, K.; Schmincke, H.-U. The role of partial melting in the 15 Ma geochemical evolution of Gran Canaria: A blob model for the Canary hotspot. *J. Petrol.* **1993**, *34*, 599–626. [\[CrossRef\]](#)
- Lundstrom, C.C.; Hoernle, K.; Gill, J. U-series disequilibria in volcanic rocks from the Canary Islands: Plume versus lithospheric melting. *Geochim. Cosmochim. Acta* **2003**, *67*, 4153–4177. [\[CrossRef\]](#)
- Geldmacher, J.; Hoernle, K.; van den Bogaard, P.; Zankl, G.; Garbe-Schönberg, D. Earlier history of the ≥ 70 -Ma-old Canary hotspot based on the temporal and geochemical evolution of the Selvagen Archipelago and neighboring seamounts in the eastern North Atlantic. *J. Volcanol. Geotherm. Res.* **2001**, *111*, 55–87. [\[CrossRef\]](#)
- Lara, L.E.; Reyes, J.; Sepúlveda, P.; Orozco, G.; Piña, M.; Becerril, L. Geología de las islas Robinson Crusoe y Santa Clara, región de Valparaíso. In *Carta Geológica de Chile*; 1 mapa escala 1:25,000; Serie Geología Básica; Servicio Nacional de Geología y Minería: Santiago, Chile, 2022; Volume 213, 42p.

24. Farley, K.A.; Basu, A.R.; Craig, H. He, Sr and Nd isotopic variations in lavas from the Juan Fernandez Archipelago, SE Pacific. *Contrib. Miner. Petrol.* **1993**, *115*, 75–87. [[CrossRef](#)]
25. Devey, C.W.; Hémond, C.; Stoffers, P. Metasomatic reactions between carbonated plume melts and mantle harzburgite: The evidence from Friday and Domingo Seamounts (Juan Fernandez chain, SE Pacific). *Contrib. Miner. Petrol.* **2000**, *139*, 68–84. [[CrossRef](#)]
26. Truong, T.B.; Castillo, P.R.; Hilton, D.R.; Day, J.M.D. The trace element and Sr-Nd-Pb isotope geochemistry of Juan Fernandez lavas reveal variable contributions from a high- $^3\text{He}/^4\text{He}$ mantle plume. *Chem. Geol.* **2018**, *476*, 280–291. [[CrossRef](#)]
27. Paquet, M.; Day, J.M.D.; Castillo, P.R. Osmium isotope evidence for a heterogeneous $^3\text{He}/^4\text{He}$ mantle plume beneath the Juan Fernandez Islands. *Geochim. Cosmochim. Acta* **2019**, *261*, 1–19. [[CrossRef](#)]
28. Reyes, J.; Lara, L.E.; Hauff, F.; Hoernle, K.; Morata, D.; Selles, D.; Cooper, O. Petrogenesis of shield volcanism from the Juan Fernández Ridge: Melting of a low-temperature pyroxenite-bearing mantle plume. *Geochim. Cosmochim. Acta* **2019**, *257*, 311–335. [[CrossRef](#)]
29. Lara, L.E.; Reyes, J.; Jicha, B.R.; Díaz-Naveas, J. $^{40}\text{Ar}/^{39}\text{Ar}$ Geochronological Constraints on the Age Progression Along the Juan Fernández Ridge, SE Pacific. *Front. Earth Sci.* **2018**, *6*, 194. [[CrossRef](#)]
30. Morales, A.J. *Geología de las Islas Robinson Crusoe y Santa Clara, Archipiélago Juan Fernández, V Región, Chile*; Universidad Católica del Norte: Antofagasta, Chile, 1987; 103p.
31. Zindler, A.; Hart, S. Chemical Geodynamics. *Annu. Rev. Earth Planet. Sci.* **1986**, *14*, 493–571. [[CrossRef](#)]
32. Hart, S.R.; Hauri, E.H.; Oschmann, L.A.; Whitehead, J.A. Mantle Plumes and Entrainment: Isotopic Evidence. *Science* **1992**, *256*, 517–520. [[CrossRef](#)]
33. Hanan, B.B.; Graham, D.W. Lead and helium isotope evidence from oceanic basalts for a common deep source of mantle plumes. *Science* **1996**, *272*, 991–995. [[CrossRef](#)] [[PubMed](#)]
34. Hauri, E.H.; Whitehead, J.A.; Hart, S.R. Fluid dynamic and geochemical aspects of entrainment in mantle plumes. *J. Geophys. Res. Solid Earth* **1994**, *99*, 24275–24300. [[CrossRef](#)]
35. Kimura, J.-I.; Gill, J.B.; Skora, S.; van Keken, P.E.; Kawabata, H. Origin of geochemical mantle components: Role of subduction filter. *Geochem. Geophys. Geosyst.* **2016**, *17*, 3289–3325. [[CrossRef](#)]
36. Hoernle, K.; Hauff, F.; Werner, R.; van den Bogaard, P.; Gibbons, A.D.; Conrad, S.; Müller, R.D. Origin of Indian Ocean Seamount Province by shallow recycling of continental lithosphere. *Nat. Geosci.* **2011**, *4*, 883–887. [[CrossRef](#)]
37. Pin, C.; Zalduegui, J.S. Sequential separation of light rare-earth elements, thorium and uranium by miniaturized extraction chromatography: Application to isotopic analyses of silicate rocks. *Anal. Chim. Acta* **1997**, *339*, 79–89. [[CrossRef](#)]
38. Simkin, T.O.M.; Smith, J.V. Minor-element distribution in olivine. *J. Geol.* **1970**, *78*, 304–325. [[CrossRef](#)]
39. Herzberg, C.; O'Hara, M.J. Plume-associated ultramafic magmas of Phanerozoic age. *J. Petrol.* **2002**, *43*, 1857–1883. [[CrossRef](#)]
40. Beattie, P. Olivine-melt and orthopyroxene-melt equilibria. *Contrib. Miner. Petrol.* **1993**, *115*, 103–111. [[CrossRef](#)]
41. Nimis, P.; Ulmer, P. Clinopyroxene geobarometry of magmatic rocks Part 1: An expanded structural geobarometer for anhydrous and hydrous, basic and ultrabasic systems. *Contrib. Miner. Petrol.* **1998**, *133*, 122–135. [[CrossRef](#)]
42. Morimoto, N. Nomenclature of Pyroxenes. *Miner. Petrol.* **1988**, *39*, 55–76. [[CrossRef](#)]
43. Le Maitre, R.W. *Igneous Rocks—A Classification and Glossary of Terms*; Cambridge University Press: Cambridge, UK, 2002; 236p. [[CrossRef](#)]
44. Irvine, T.N.; Baragar, R.A. A guide to the chemical classification of the common volcanic rocks. *Can. J. Earth Sci.* **1971**, *8*, 523–548. [[CrossRef](#)]
45. Gerlach, D.C.; Hart, S.R.; Morales, V.W.J.; Palacios, C. Mantle heterogeneity beneath the Nazca plate: San Felix and Juan Fernandez islands. *Nature* **1986**, *322*, 165–169. [[CrossRef](#)]
46. Baker, P.E.; Gledhill, A.; Harvey, P.K.; Hawkesworth, C.J. Geochemical evolution of the Juan Fernandez Islands, SE Pacific. *J. Geol. Soc. London* **1987**, *144*, 933–944. [[CrossRef](#)]
47. Willbold, M.; Stracke, A. Trace element composition of mantle end-members: Implications for recycling of oceanic and upper and lower continental crust. *Geochem. Geophys. Geosyst.* **2006**, *7*, Q04004. [[CrossRef](#)]
48. Sun, S.; McDonough, W.F. Chemical and isotopic systematics of oceanic basalts: Implications for mantle composition and processes. *Geol. Soc. London Spec. Publ.* **1989**, *42*, 313–345. [[CrossRef](#)]
49. Hart, S.R. A large-scale isotope anomaly in the Southern Hemisphere mantle. *Nature* **1984**, *309*, 753–757. [[CrossRef](#)]
50. Ghiorso, M.S.; Sack, R.O. Chemical mass-transfer in magmatic processes IV. A revised and internally consistent thermodynamic model for the interpolation and extrapolation of liquid-solid equilibria in magmatic systems at elevated-temperatures and pressures. *Contrib. Mineral. Petrol.* **1995**, *119*, 197–212. [[CrossRef](#)]
51. Asimow, P.D.; Ghiorso, M.S. Algorithmic modifications extending MELTS to calculate subsolidus phase relations. *Am. Mineral.* **1998**, *83*, 1127–1132. [[CrossRef](#)]
52. Smith, P.M.; Asimow, P.D. *Adiabat_1ph*: A new public front-end to the MELTS, pMELTS, and pHMELTS models. *Geochem. Geophys. Geosyst.* **2005**, *6*, Q02004. [[CrossRef](#)]
53. Kimura, J.-I.; Ariskin, A.A. Calculation of water-bearing primary basalt and estimation of source mantle conditions beneath arcs: PRIMACALC2 model for WINDOWS. *Geochem. Geophys. Geosyst.* **2014**, *15*, 1494–1514. [[CrossRef](#)]
54. Dixon, J.E.; Leist, L.; Langmuir, C.; Schilling, J.-G. Recycled dehydrated lithosphere observed in plume-influenced mid-ocean-ridge basalt. *Nature* **2002**, *420*, 385–389. [[CrossRef](#)] [[PubMed](#)]

55. Jackson, M.G.; Halldórsson, S.A.; Price, A.; Kurz, M.D.; Konter, J.G.; Koppers, A.A.P.; Day, J.J.D. Contrasting old and young volcanism from Aitutaki, Cook Islands: Implications for the origins of the Cook-Austral Volcanic Chain. *J. Petrol.* **2020**, *61*, ega037. [[CrossRef](#)]
56. Konter, J.G.; Staudigel, H.; Blichert-Toft, J.; Hanan, B.B.; Polvé, M.; Davies, G.R.; Shimizu, N.; Schiffman, P. Geochemical stages at Jasper seamount and the origin of intraplate volcanoes. *Geochem. Geophys. Geosyst.* **2009**, *10*, Q02001. [[CrossRef](#)]
57. Jackson, M.G.; Shirey, S.B. Re-Os isotope systematics in Samoan shield lavas and the use of Os-isotopes in olivine phenocrysts to determine primary magmatic compositions. *Earth Planet. Sci. Lett.* **2011**, *312*, 91–101. [[CrossRef](#)]
58. Dixon, J.; Clague, D.A.; Cousens, B.; Monsalve, M.L.; Uhl, J. Carbonatite and silicate melt metasomatism of the mantle surrounding the Hawaiian plume: Evidence from volatiles, trace elements, and radiogenic isotopes in rejuvenated-stage lavas from Niihau, Hawaii. *Geochem. Geophys. Geosyst.* **2008**, *9*, Q09005. [[CrossRef](#)]
59. Mallick, S.; Kuhl, S.E.; Saal, A.E.; Klein, E.M.; Bach, W.; Monteleone, B.D.; Boesenberg, J.S. Evidence of South American lithosphere mantle beneath the Chile mid-ocean ridge. *Earth Planet. Sci. Lett.* **2023**, *620*, 118320. [[CrossRef](#)]
60. Klein, E.M.; Karsten, J.L. Ocean-ridge basalts with convergent-margin geochemical affinities from the Chile Ridge. *Nature* **1995**, *375*, 52–57. [[CrossRef](#)]
61. Macdougall, J.D.; Lugmair, G.W. Extreme isotopic homogeneity among basalts from the southern East Pacific Rise: Mantle or mixing effect? *Nature* **1985**, *313*, 209–211. [[CrossRef](#)]
62. Chauvel, C.; Maury, R.C.; Blais, S.; Lewin, E.; Guillou, H.; Guille, G.; Rossi, P.; Gutscher, M. The size of plume heterogeneities constrained by Marquesas isotopic stripes. *Geochem. Geophys. Geosyst.* **2012**, *13*, Q07005. [[CrossRef](#)]
63. Guillou, H.; Maury, R.C.; Guille, G.; Chauvel, C.; Rossi, P.; Pallares, C.; Legendre, C.; Blais, S.; Liorzou, C.; Deroussi, S. Volcanic successions in Marquesas eruptive centers: A departure from the Hawaiian model. *J. Volcanol. Geotherm. Res.* **2014**, *276*, 172–188. [[CrossRef](#)]
64. Homrighausen, S.; Hoernle, K.; Geldmacher, J.; Wartho, J.; Hauff, F.; Portnyagin, M.; Werner, R.; van den Bogaard, P.; Garbe-Schönberg, D. Unexpected HIMU-type Late-Stage Volcanism on the Walvis Ridge. *Earth Planet. Sci. Lett.* **2018**, *492*, 251–263. [[CrossRef](#)]
65. Borisova, A.Y.; Tilhac, R. Derivation of Hawaiian rejuvenated magmas from deep carbonated mantle sources: A review of experimental and natural constraints. *Earth-Sci. Rev.* **2021**, *222*, 103819. [[CrossRef](#)]
66. Othman, D.B.; Polvé, M.; Allègre, C.J. Nd-Sr isotopic composition of granulites and constraint on the evolution of the lower continental crust. *Nature* **1984**, *307*, 510. [[CrossRef](#)]
67. Weaver, B.L. The origin of ocean island basalt end-member compositions: Trace element and isotopic constraints. *Earth Planet. Sci. Lett.* **1991**, *104*, 381–397. [[CrossRef](#)]
68. Roy-Barman, M.; Allègre, C.J. 187Os/186Os in oceanic island basalts: Tracing oceanic crust recycling in the mantle. *Earth Planet. Sci. Lett.* **1995**, *129*, 145–161. [[CrossRef](#)]
69. Rehkämper, M.; Hofmann, A.W. Recycled ocean crust and sediment in Indian Ocean MORB. *Earth Planet. Sci. Lett.* **1997**, *147*, 93–106. [[CrossRef](#)]
70. Blichert-Toft, J. Hf isotope evidence for pelagic sediments in the source of hawaiian basalts. *Science* **1999**, *285*, 879–882. [[CrossRef](#)] [[PubMed](#)]
71. Stracke, A.; Hofmann, A.W.; Hart, S.R. FOZO, HIMU, and the rest of the mantle zoo. *Geochem. Geophys. Geosyst.* **2005**, *6*, Q05007. [[CrossRef](#)]
72. Ribe, N.M.; Christensen, U.R. The dynamical origin of Hawaiian volcanism. *Earth Planet. Sci. Lett.* **1999**, *171*, 517–531. [[CrossRef](#)]
73. Legendre, C.; Maury, R.C.; Blais, S.; Guillou, H.; Cotton, J. Atypical hotspot chains: Evidence for a secondary melting zone below the Marquesas (French Polynesia). *Terra Nova* **2006**, *18*, 210–216. [[CrossRef](#)]

Disclaimer/Publisher’s Note: The statements, opinions and data contained in all publications are solely those of the individual author(s) and contributor(s) and not of MDPI and/or the editor(s). MDPI and/or the editor(s) disclaim responsibility for any injury to people or property resulting from any ideas, methods, instructions or products referred to in the content.